Interpreting Chemical Enhancements of Surface-enhanced Raman Scattering

Ran Chen[1] and Lasse Jensen[1, a)]

Department of Chemistry, Pennsylvania State University, University Park, Pennsylvania 16802, United States

(Dated: 30 August 2023)

Surface-enhanced Raman scattering (SERS) provides orders of magnitude of enhancements to weak Raman scattering. The improved sensitivity and chemical information conveyed in the spectral signatures make SERS a valuable analysis technique. Most of SERS enhancements come from the electromagnetic enhancement mechanism, and changes in spectral signatures are usually attributed to the chemical enhancement mechanism. As the electromagnetic mechanism has been well studied, we will give an overview of models related to the chemical mechanism, which explain the Raman response in terms of electronic transitions or induced electron densities. In the first class of models based on electronic transitions, chemical enhancements are attributed to changes in transitions of the molecule and new charge-transfer transitions. The second class of models relate chemical enhancements to charge flows near the molecule-metal interface by partitioning the induced electron density of the SERS system in real space. Selected examples will be given to illustrate the two classes of models, and connections between the models are demonstrated for prototypical SERS systems.

[a)]Electronic mail: jensen@chem.psu.edu

I. INTRODUCTION

Raman intensities can be significantly enhanced when molecules are in proximity to nanostructured metal surfaces. This phenomenon was discovered decades ago and is known as surface-enhanced Raman scattering (SERS).[1–3] Large SERS enhancements have been observed in various systems,[4–19] and single molecule detection using SERS has been reported.[20–34] In addition to its high sensitivity, SERS allows for chemical-specific, non-destructive, and label-free analysis.[32,35–45] These characteristics make SERS a valuable tool for identifying molecular species and structures in diverse fields such as biology,[46–56] materials science,[39,57,58] and surface chemistry.[59–66]

To understand SERS enhancement mechanisms, we start from the process of normal Raman scattering (NRS), which is shown in Fig.1(a). In the diagram, the solid lines represent the vibronic states of an unbound molecule, and the dashed line represents the virtual state of the molecule. The blue and green arrows represent the absorption and emission processes, respectively. The lengths of the arrows represent the frequencies of the incident and scattered light. Raman scattering happens when the energy difference between the incident and scattered light matches the energy gap between the initial and final vibronic states. The Raman intensity can be enhanced when the molecule is adsorbed on a metal surface, and the enhancement mechanisms are explained in Fig.1(b) to (e). The density of states of the metal surface is represented by the block on the left side of each diagram. The valence and conduction bands of the metal surface are represented by the colored and uncolored blocks, respectively. Most of the enhancement usually arises from the surface plasmon resonance of the metal surface. This mechanism is called the electromagnetic mechanism (EM) and is illustrated in Fig.1(b). In the early studies of SERS, the surface plasmon resonance has been considered to explain enhancements.[67–79] At the surface plasmon resonance, conduction electrons collectively oscillate at the metal surface. The freely propagating incident light is confined to an enhanced local field near the metal surface at the resonance frequency. The enhanced local field is labeled as F in Fig.1(b). The absorption and emission transitions of the adsorbed molecule are enhanced due to the enhanced local field. The enhanced transitions are represented as bolded arrows. The SERS enhancement scales with the local field enhancement to the fourth power approximately.[74,80] More careful evaluation of the SERS enhancement considers other factors such as the field gradient effect, and the frequency difference between the incident and scattered light.[39,69,77,80–100] For materials other than metal, when particle sizes are comparable

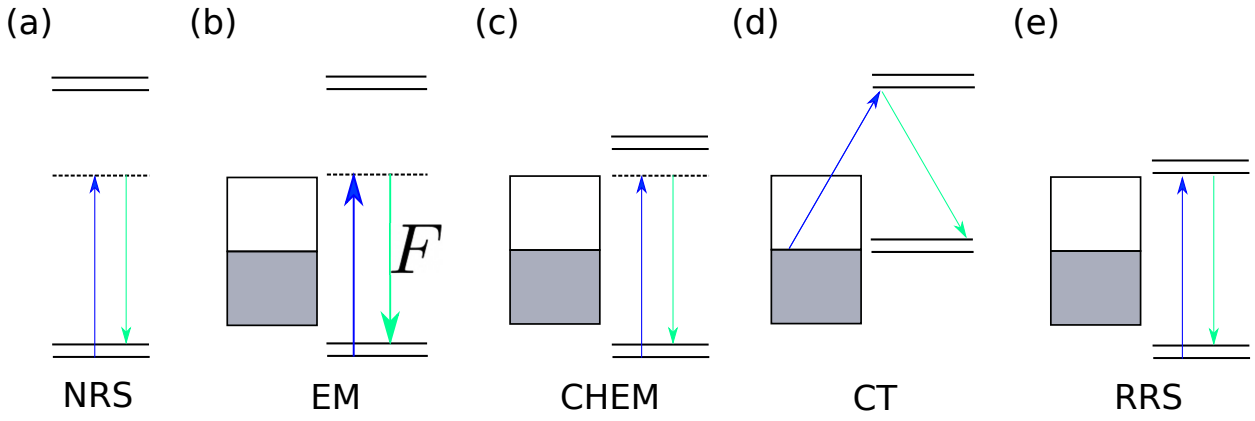

FIG. 1. A diagram of normal Raman scattering (NRS) is shown in (a). Different enhancement mechanisms of SERS are illustrated: electromagnetic mechanism (EM) in (b), static chemical mechanism (CHEM) in (c), charge-transfer mechanism (CT) in (d), and resonance Raman scattering mechanism (RRS) in (e).

to the wavelength of the incident light, Mie resonance can give rise to enhanced local fields and promote Raman scattering.[101–104]

Other enhancement sources are due to chemical bonding between the molecule and the surface, which are grouped as the chemical mechanism (CM).[69,105–107] Chemical enhancements generally are orders of magnitude weaker than electromagnetic enhancements, but understanding CM is extremely important for extracting chemical information of molecule-metal interfaces from SERS spectra. The importance of CM has been emphasized in the early studies of SERS. For example, SERS enhancements of CO and N_2 differ by a factor of 200 under the same experimental conditions, and SERS enhancements show potential-dependence in electrochemical experiments.[106,108–112] Understanding CM is also important for explaining SERS enhancements when the curvature of the metal surface approaches a few nanometers or less. Tip-enhanced Raman scattering (TERS) is a good example, where a sharp metal tip with a nanometer-sized apex is applied in a scanning microscopy setup.[32,113–123] In such case, electron tunneling across metal junctions or between molecules and metal can make enhancements different from EM predictions.[124–138] Therefore, the understanding of CM is indispensable in TERS applications such as imaging molecular vibrations with high-resolution[139–146] and characterizing surfaces and reactions.[58,140,147–153] Chemical enhancements can also become dominant when the surface plasmon resonance is absent such as for semiconductor substrates.[101,103,154–172] Semiconductor substrates can provide selective SERS enhancements, good biocompatibility, good reproducibility, and low manufacturing cost, and SERS applications have been extended due to the advantages of

the semiconductor substrates.[173–184] As significant effort has been made to develop semiconductor SERS substrates, the understanding of CM should be emphasized.

Studies of CM can be traced back to the early studies of SERS where molecular resonance and charge-transfer resonance were suspected to contribute to SERS enhancements.[3,69,185–187] The possible involvement of the charge-transfer states in SERS was supported experimentally by Avouris and Demuth, who identified electronic excitations related to molecule-metal charge transfer using electron energy-loss spectroscopy (EELS).[188] A similar investigation was conducted later by the Campion group and the Moskovits group.[189,190] Adrian explained that the charge-transfer states were formed because of the orbital overlap between molecules and surfaces, and the photon-induced charge transfer can contribute to SERS enhancements.[191] Arenas, Otero, and other groups pointed out that adsorbed molecules can form transient radicals because of charge transfer, and vibrations connecting electronic states of the molecules and radicals tend to be enhanced.[26,111,192–202] Persson derived a model of Raman scattering for chemisorbed molecules based on the Newns-Anderson model[203], and showed how charge transfer excitations can contribute to SERS enhancements.[204] An adatom model constructed by Otto and other groups[205–218] pointed out that atomically rough surfaces promote molecule-metal charge transfer by increasing electron-phonon coupling and avoiding electron–hole excitations at the interface. The importance of the nanoscale surface roughness is also emphasized by EM. In EM, compared with flat surfaces, local fields on rough surfaces are more enhanced and provide larger SERS enhancements. More recently, CM has been studied on a system-by-system basis using electronic structure methods under well-defined conditions, as chemical enhancements are highly system specific. Various factors influencing SERS enhancements can be investigated, such as molecule-metal bonding, surface roughness, incident light frequencies, and vibrational patterns. Time-dependent Hartree-Fock calculations using metal clusters were applied by Schatz and coworkers to study SERS of H_2 on Li surfaces.[219,220] In recent studies, density functional theory (DFT) calculations with molecules on localized clusters[105,125,221–242] or periodic slabs[157,243–246] have been applied. Multiple models have been developed to interpret chemical enhancements based on the electronic structures of the simulated systems. The findings of the CM studies can be summarized to three enhancement contributions: the static chemical interaction (CHEM), charge-transfer resonance (CT), and molecular resonance scattering (RRS).[107] CHEM is illustrated in Fig.1(c), where the energy gap between the ground state and the excited states of the molecule is decreased when the molecule is bound to the surface. The narrowed gaps increase the molecular polarizability and the Raman intensity. CT

is illustrated in Fig.1(d), where the absorption or emission transition happens between the Fermi level of the surface and the molecular states. The CT transition does not exist for the unbound molecule, and the new CT transition leads to an extra contribution to the Raman intensity. The enhancement can also arise from RRS, which is illustrated in Fig.1(e). Because the molecule-metal bonding decreases the energy gap between the ground state and the excited states of the molecule, the absorption transition reaches an excited state rather than the virtual state. The Raman intensity is enhanced as the transition to a real excited state provides a larger contribution to the Raman intensity than the virtual state.

It should be emphasized that the CHEM enhancement defined in this work does not correspond to all non-plasmonic enhancement and only corresponds to the enhancement contribution from the ground state bonding between the molecule and the metal. CHEM describes spectral changes caused by the ground state chemical interaction between the molecule and the metal, which is not associated with any photon excitations of the system. The collective non-plasmonic enhancement in this work is called the chemical enhancment, and the corresponding mechanism is called the chemical mechanism (CM). CM includes enhancement contributions from the ground state bonding between the molecule and the metal (CHEM), the photon-induced charge transfer between the molecule and the metal (CT), and the resonance Raman scattering of the molecule (RRS). CT and RRS result in Raman enhancements through the resonance Raman effect, when the laser frequency matches the CT or molecular excitations.

In this review, we will give an overview of models that explain chemical enhancements of SERS based on electronic structure simulations. The models interpret chemical enhancements by partitioning the Raman response in terms of electronic transitions or relating chemical enhancements to charge flows near the molecule-metal interface. Key insights of the models will be illustrated, and connections between the models will be demonstrated.

II. THE TRANSITION-BASED INTERPRETATION

A. A TWO-STATE MODEL

An accurate description of electronic and vibrational states of SERS systems is required for modeling chemical enhancements using electronic structure methods. However, when interpreting chemical enhancements, considering full electronic structures of the SERS systems is not

practical. A relatively simple interpretation can be constructed by mapping simulation or even experimental spectra to simple models. Here, we first introduce a two-state model, which provides a simple explanation of chemical enhancements at the static limit.[157,222,224,243,244] The polarizability derivative of a two-state system can be expressed as[222]

$$\frac{\partial \alpha_{ab}}{\partial Q_k} = -\frac{\mu_a \mu_b}{\omega^2}\left(\frac{\partial \omega}{\partial Q_k}\right), \tag{1}$$

where α is the electronic polarizability tensor and a, b are Cartesian directions. μ is the electronic transition dipole moment and ω is the corresponding excitation energy. Q_k is a vibrational mode of the system. Because the Raman intensity is proportional to the square of the polarizability derivative with respect to the vibration, the enhancement factor (EF) of an adsorbed molecule will be

$$\mathrm{EF} \propto \left(\frac{\omega_X}{\omega_e}\right)^4 \left(\frac{\mu_{e,a}\mu_{e,b}}{\mu_{X,a}\mu_{X,b}}\right)^2 \left(\frac{\partial \omega_e}{\partial Q_k}\right)^2 \left(\frac{\partial \omega_X}{\partial Q_k}\right)^{-2} \propto \left(\frac{\omega_X}{\omega_e}\right)^4, \tag{2}$$

where ω_X is lowest excitation energy of the molecule, and ω_e is the lowest CT excitation energy of the SERS system. μ_X and μ_e are the corresponding transition dipole moments. Q_k is the vibrational mode. The chemical enhancement scales roughly with the excitation energy ratio to the fourth power between the SERS system and the molecule. The excitation energies can be evaluated by response calculations and can also be approximated by the ground state electronic structures. For example, the lowest excitation energy of the molecule can be approximated by the energy gap between the highest occupied molecular orbital (HOMO) and the lowest unoccupied molecular orbital (LUMO) of the molecule. The lowest CT excitation energy of the SERS system can be approximated by the energy gap between the frontier orbitals of the molecule and the metal. Thus, the two-state model points out that adsorbed molecules with significant stabilization of the HOMO-LUMO gaps are likely to have large chemical enhancements. This is consistent with the fact that aromatic molecules are usually found to be strongly SERS active. The two-state model also shows that CHEM and CT mechanisms both stem from the CT excitation between the molecule and the metal.

A pyridine-Ag_{20} complex from the work by the Jensen group is discussed as an example,[222] and the structure diagram of the complex is shown in Fig.2(a). The alignment of the states showed that the lowest CT transition would happen between the HOMO of the cluster and the LUMO of the molecule, which are plotted in Fig.2(a) with the structure diagram of the system. When approximating the CT energy with the ground state electronic structure, the energy gaps between orbitals containing the frontier orbitals were weight averaged due to orbital mixing between the molecule

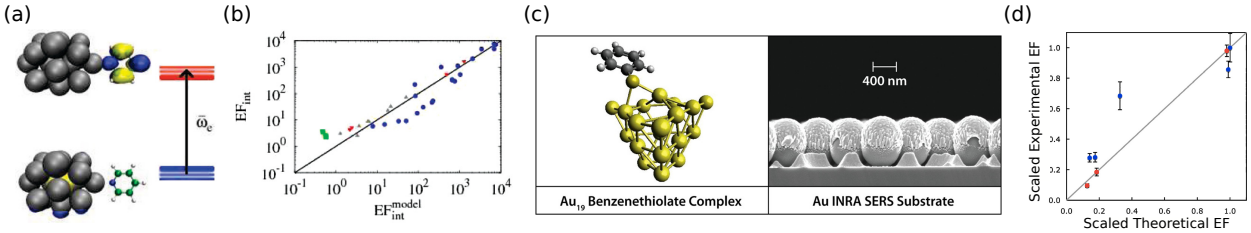

FIG. 2. (a) The structure diagrams of a pyridine-Ag_{20} complex from Ref. 222 with the HOMO of the cluster and the LUMO of the molecule. (b) The integrated enhancement factors (EF_{int}) of the studied systems from Ref. 222 are plotted versus the integrated enhancements factors calculated using the two-state model (EF_{int}^{model}). Reproduced with permission from J. Am. Chem. Soc, 131, 4090, (2009). Copyright 2009 American Chemical Society (c) The structure diagram of a benzenethiolate-Au_{19} complex and the SEM image of the gold substrate from Ref. 224. (d) Scaled experimental enhancement factors are plotted versus the scaled simulated enhancement factors for the benzenethiolate systems from Ref. 224 . Reproduced with permission from J. Phys. Chem. Lett., 4, 2599 (2013). Copyright 2013 American Chemical Society

and the metal. The blue and red lines in the diagram represent the orbitals containing the HOMO of the cluster and the LUMO of the molecule, respectively. $\bar{\omega}_e$ in the diagram is the approximate charge transfer energy. To test the two state model, the Jensen group studied pyridine derivatives, benzenethiols, and other small molecules on Ag clusters. The integrated enhancements estimated by the two-state model and simulated by time-dependent density functional theory (TDDFT) are compared in Fig.2(b). Fig.2(b) shows a good correlation between the estimated enhancements by the two-state model and the simulated enhancements by TDDFT. The correlation indicates that the integrated enhancements for these systems were well described by the two-state model. Among these systems, the Jensen group found that the donor groups tended to increase the CT gaps and decrease the enhancements, whereas the acceptor groups tended to decrease the CT gaps and increase the enhancements. Thus, by approximating the excitation energies by the orbital gaps, the two-state model allows chemists to utilize the chemical intuition about molecule-metal bonding to estimate the enhancements between different molecules before running response calculations. The two-state model was further verified by Van Duyne, Schatz and coworkers experimentally.[224] They studied substituted benzenethiols on Ag and Au surfaces. Fig.2(c) shows a structure diagram of the simulated model system and a scanning electron microscope (SEM) image of the gold substrate used in the experiment. The flat and smooth gold substrate used in the experiment provided uniform EM enhancements over large areas, which allowed for an investigation of CM

independently of EM. Simulated enhancements are plotted versus experimental enhancements in Fig.2(d) for the ring stretching modes near 1600 cm^{-1} of the benzenethiol molecule on the gold surface. The good correlation between the simulated and experimental enhancements indicates that TDDFT was reasonably accurate in calculating relative enhancements. Then, the estimated enhancements by the two-state model were showed to agree with the simulated enhancements by TDDFT. Therefore, the estimated enhancements by the two-state model were shown to agree with the experimental enhancements. Among the studied systems, Van Duyue, Schatz and coworkers showed that stronger electron donating groups on the benzene unit led to higher enhancements. Zayak and coworkers also applied the two-state model to compare enhancements among vibrations for a benzenethiol-Au system.[243] The relative enhancement was plotted for each vibration versus the geometric derivative of the CT gap, named the deformation potential. A good correlation between the relative enhancements and the deformation potentials was found for most of the vibrations. This is consistent with the approximation of the two-state model that the Franck–Condon (FC) term is considered and the Herzberg–Teller (HT) term is neglected. The justification for this approximation is that the largest variation of integrated enhancements between different molecules is expected to be due to the excitation energy changes.

B. A UNIFIED VIEW OF SERS

To develop a general model explaining all enhancement contributions, Lombardi and Birke derived a single expression of SERS including surface plasmon resonance, CT resonance, and molecular resonance based on the HT coupling.[109,247–252] The model shows that the three types of resonances are intimately linked by the HT coupling and cannot be considered separately. The model was named as a unified view of SERS. In this model, the Raman polarizability of a SERS system is expressed as a sum of A, B, and C terms. The A term corresponds to the FC contribution, and the B and C terms correspond to the HT contribution. The difference between the B and C terms is that the B term contains the molecule-to-metal charge transfer, while the C term contains the metal-to-molecule charge transfer. The importance of the A, B, and C terms was compared by Lombardi, Birke, and other groups.[250,252–255] The studies showed that the A term contributed to Raman intensities of symmetric vibrations, while the B and C terms contributed to Raman intensities of both symmetric and asymmetric vibrations. The A term only became dominant when the system was near resonance, while the B and C terms were important at all

resonance conditions. Thus, the B and C terms were usually considered when explaining SERS selection rules.[256–260] The importance of the charge transfer states in the B and C terms has also been emphasized because the CT states usually have lower energies than the molecular excited states.[109,201,252,256] For example, Lombardi and coworkers pointed out that as the excitation frequency scanned through the CT resonance, the enhancements of asymmetric vibrations relative to symmetric vibrations would vary, while in the absence of the CT resonance, the relative enhancements of both types of vibrations would be the same regardless of the excitation frequency.[252] Before we discuss the unified view of SERS in detail, it is worth noting that attempts of building a general theory of SERS[6,7,81,261–266] or assigning SERS enhancements to CT resonance using the HT coupling framework[108,267–275] have also been made by other groups.

To demonstrate how the HT coupling links different kinds of resonance, the C term is examined

$$R_{IFK} = \frac{\mu_{KI}\mu_{FK}h_{IF}\langle i|Q_k|f\rangle}{((\varepsilon_1+2\varepsilon_0)^2+\varepsilon_2^2)(\omega_{FK}^2-\omega^2+\gamma_{FK}^2)(\omega_{IK}^2-\omega^2+\gamma_{IK}^2)}\,, \tag{3}$$

where I, K are the ground state and excited electronic states of the molecule. F is the Fermi level of the metal. i and f are the initial and final vibrational states. The three terms in the denominator depict three different resonance contributions to the SERS enhancement. ω is the frequency of the incident light. The metal is assumed to have continuous states, and its response is approximated by a complex dielectric function $\varepsilon_1 + i\varepsilon_2$ where ε_1 and ε_2 are the real and imaginary parts of the metal dielectric function. The first term in the denominator corresponds to the plasmon resonance at the frequency where $\varepsilon_1 = -2\varepsilon_0$, and ε_0 is the real part of the dielectric function of the surrounding medium. The other two terms in the denominator correspond to the CT resonance at ω_{FK} and the molecular resonance at ω_{IK}. γ_{FK}, and γ_{IK} are the damping parameters of the CT resonance and molecular resonance, respectively. The terms in the numerator determine SERS selection rules. $\langle i|Q_k|f\rangle$ requires normal harmonic oscillator selection rules. The molecular and CT transitions labeled as μ_{IK} and μ_{FK}, respectively, need to be nonzero for the vibration to be SERS active. Since the most significant local field due to the plasmon resonance is normal to the metal surface, components of the transition dipole moments normal to the surface are expected to be most enhanced, which is known as the surface selection rule. The HT coupling term between states I and F, h_{IF}, allows intensity borrowing between the molecular transition μ_{IK} and the charge transfer transition μ_{FK}. The excitation energies of the three kinds of resonance and the corresponding dipole moments can be obtained from absorption spectra of the molecule-metal system. The HT coupling term is difficult to measure experimentally, but electronic structure simulations may prove to be

useful in this regard.[276]

To illustrate how the unified view of SERS explains SERS selection rules, a pyridine-Ag system is discussed as an example.[250,252] Pyridine is known to have C_{2v} symmetry, and the pyridine-Ag system was assumed to retain the symmetry. In the pyridine-Ag system, vibrations of a_1 and b_2 symmetry were SERS active while vibrations of b_1 and a_2 symmetry were SERS inactive.[252] The unified view of SERS pointed out that the CT transition could contribute to the enhancements by intensity borrowing from nearby molecular transitions through the HT coupling. Thus, the SERS selection rules of the pyridine-Ag system can be explained by examining the symmetry of the CT transition and the borrowed molecular transitions. Given the symmetry of the pyridine-Ag system and the surface selection rule, the charge transfer transition was deduced to have A_1 symmetry. The low-lying molecular transitions borrowed by the CT transition were found to have symmetry of A_1, B_1, and B_2. Thus the SERS active vibrations would have symmetry of a_1, b_1, and b_2. Because the borrowed transitions of B_1 symmetry were weak, the vibrations of b_1 symmetry were relatively less enhanced. Thus the main peaks in the SERS spectra of the pyridine-Ag system corresponded to the vibrations of a_1 and b_2 symmetry. The analysis can be applied to molecules with different symmetry and orientations on the surface. Besides being able to explain SERS selection rules, the unified view of SERS can also provide a strategy of optimizing the sensitivity of SERS substrates by taking advantage of coupling different kinds of resonance.[161,174,257–260,277–287]

The B and C terms can also be explained visually, and diagrams explaining the B and C terms are shown in Fig.3(a).[252] The diagrams show that the molecular transition μ_{IK} exists for both B and C terms. For the B term, the CT transition, μ_{IF}, happens from the molecule to the metal, and the HT coupling term, h_{FK}, connects the Fermi level and the molecular excited state. For the C term, the CT transition, μ_{FK}, happens from the metal to the molecule, and the HT coupling term, h_{IF}, connects the molecular ground state and the Fermi level.

Lombardi and Birke also extended the unified view of SERS to semiconductor substrates, where the CT transitions terminate at band edges rather than the Fermi level.[101,103,156] For example, the term R_{IFK} discussed above is changed to

$$R_{IVK} = \frac{\mu_{VK}\mu_{KI}h_{IV}\langle i|Q_k|f\rangle}{((\varepsilon_1+2\varepsilon_0)^2+\varepsilon_2^2)(\omega_{VK}^2-\omega+\gamma_{VK}^2)(\omega_{KI}^2-\omega^2+\gamma_{KI}^2)}\,, \tag{4}$$

where V is the edge of the valence band of the semiconductor substrate, and h_{IV} is the HT coupling term between the valence band edge and the excited state of the molecule. γ_{VK} is the damping parameter of the charge transfer transition at ω_{VK}. An extra term emerges to include the exciton

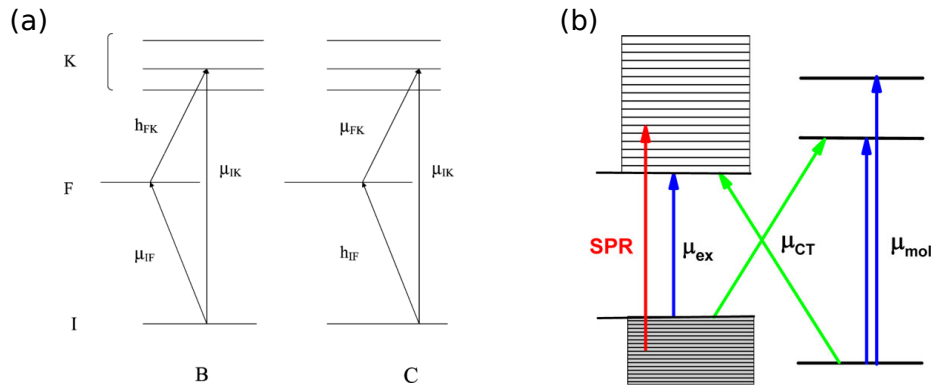

FIG. 3. Diagrams of transitions for a molecule-metal system from Ref. 252 are plotted in (a). Reproduced with permission from J. Phys. Chem. C, 112, 5605 (2008). Copyright 2008 American Chemical Society A diagram of transitions for a molecule-semiconductor system from Ref. 103 is plotted in (b). Reproduced with permission from J. Phys. Chem. C, 118, 11120 (2014). Copyright 2014 American Chemical Society

transition in the semiconductor.

$$R_{KVC} = \frac{\mu_{CV}\mu_{VK}h_{KC}\langle i|Q_k|f\rangle}{((\varepsilon_1+2\varepsilon_0)^2+\varepsilon_2^2)(\omega_{VK}^2-\omega+\gamma_{VK}^2)(\omega_{CV}^2-\omega^2+\gamma_{CV}^2)}\,, \tag{5}$$

where C is the edge of the conduction band of the semiconductor substrate. ω_{CV} and γ_{CV} are the resonance frequency and the damping parameter of the exciton transition.

SERS selection rules of molecules on semiconductor substrates can be explained by the symmetry of the CT transitions, molecular transitions, and exciton transitions.[101,156,277] Similarly, the unified view of SERS for semiconductor substrates can be visually explained in a transition diagram of a molecule-semiconductor system shown in Fig.3(b).[103] The lines on the left and right sides of the diagram represent the electronic states of the semiconductor surface and the molecule, respectively. The surface plasmon resonance is represented by the red arrow, and the exciton excitation is represented by the blue arrow on the left side. The charge transfer transitions are represented by the green arrows, and the molecular transitions are represented by the blue arrows on the right side.

C. A SEMIEMPIRICAL MOLECULAR ORBITAL METHOD

The unified view of SERS shows that different kinds of resonance contribute together to SERS enhancements. It is challenging to determine the relative enhancement contributions of various mechanisms. For example, the CHEM enhancement has been approximated as the enhancement

at the static limit, and the EM enhancement has been estimated as the enhancement ratio at the plasmon resonance versus the static limit.[221] However, this approximation requires the excitation frequencies of different kinds of resonance to be well separated, and the approximation neglects the non-resonant EM enhancement.

To separate chemical and electromagnetic enhancements, a semiempirical configuration interaction method with single excitations based on the Intermediate Neglect of Differential Overlap Hamiltonian (INDO/SCI)[288–290] was developed by Gieseking and Schatz.[225–227,291] INDO/SCI can be applied to calculate the electronic structures of SERS systems, and the frequency-dependent polarizabilities of the studied systems can be computed using a sum-over-state formula with the INDO/SCI states. In INDO/SCI, the interaction between atomic orbitals on different atoms is determined as

$$H_{\mu\nu}^{AB} = \frac{\beta_{\mu}^{A} + \beta_{\nu}^{B}}{2} S_{\mu\nu} \quad , \tag{6}$$

where μ and ν are atomic orbitals on atom A and B respectively. $S_{\mu\nu}$ is the orbital overlap between orbitals μ and ν. β_{μ}^{A} and β_{ν}^{B} are parameters controlling the interaction strength, which can be fitted against experimental or simulated absorption spectra.[292]

As chemical enhancements arise from the orbital overlap between the molecule and the metal, chemical enhancements can be eliminated if the orbitals of the molecule and the metal are not allowed to interact. An INDO parameter set, INDO-EM, neglects the orbital overlap between the molecule and the metal and forbids both ground state and induced charge transfer between the two moieties. Thus, only electromagnetic enhancements are considered using the INDO-EM parameter set, provided that no molecular resonance is excited. Enhancement differences calculated using the standard INDO and the INDO-EM parameter sets lead to chemical enhancements.

To demonstrate the application of INDO/SCI, a pyridine-Ag_{20} complex is discussed in Fig.4.[227] INDO/SCI was shown to provide a straightforward decomposition of the enhancements at different excitation energies into electromagnetic and chemical contributions. The total and decomposed enhancements of the pyridine-Ag_{20} complex are plotted versus the excitation energies in Fig.4(a). The solid, dotted, and dashed lines represent the total, electromagnetic, and chemical enhancements, respectively. The decomposition result showed that the electromagnetic enhancements were at the order of 10 when the surface plasmon was off resonance and were increased to the order of 100 to 1000 when the surface plasmon was on resonance. Meanwhile, the chemical enhancements were at the order of 10 when the system was off resonance and were increased to the order of 100 when the CT resonance was excited.

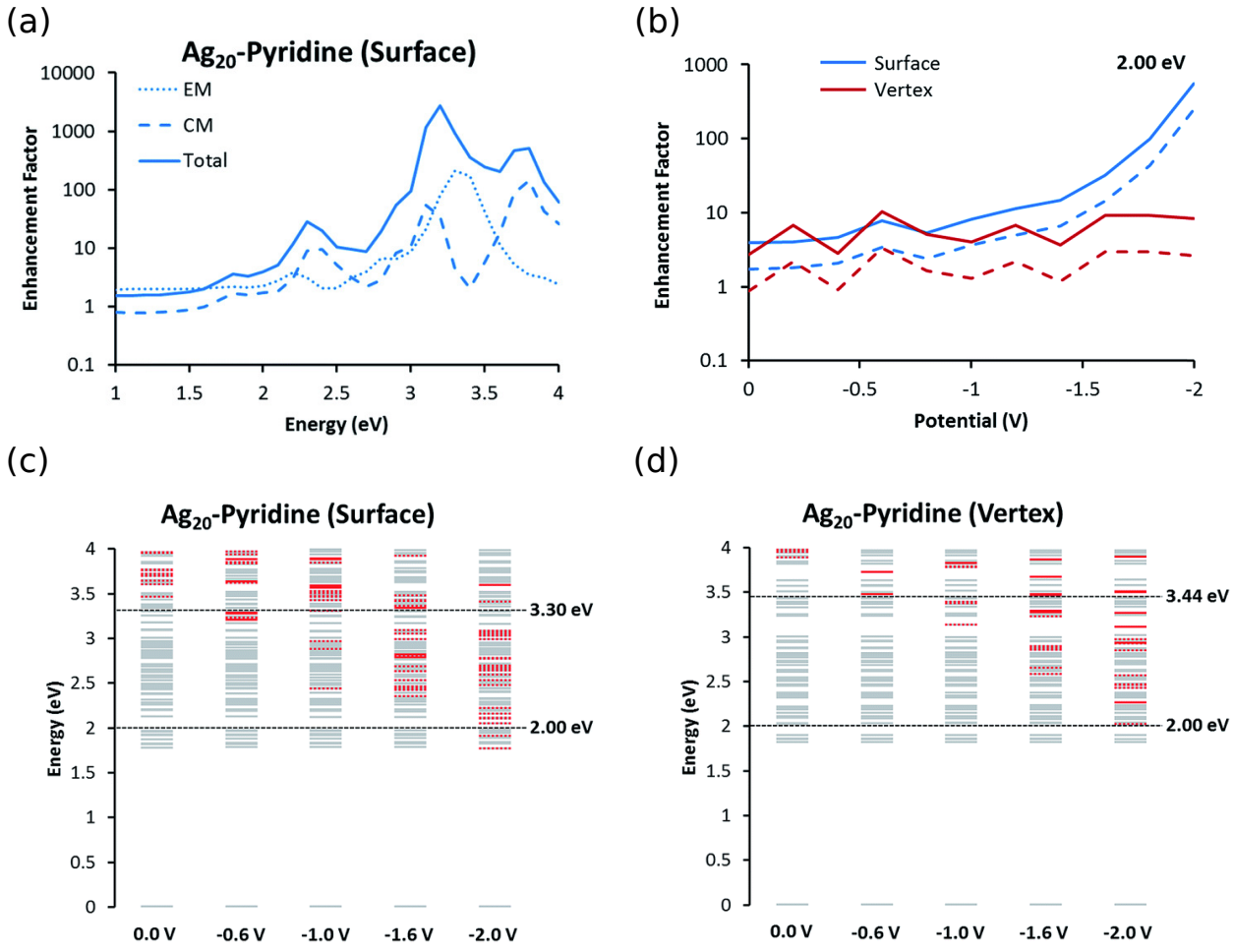

FIG. 4. Enhancements of a pyridine-Ag_{20} system are decomposed and plotted versus the incident light energies in (a). Enhancements at 2.00 eV of the pyridine-Ag_{20} system with surface and vertex binding configurations are decomposed and plotted versus the applied potentials in (b). Excited state energies at the INDO/SCI level for the pyridine-Ag_{20} system with surface and vertex binding configurations are plotted versus the applied potentials in (c) and (d). Figures adapted from Ref.[227] Reproduced with permission from Faraday Discuss 205, 149 (2017). Copyright 2017 Royal Society of Chemistry.

INDO/SCI was also shown to explain the effects of applied potentials and binding configurations on enhancements. The total and decomposed enhancements at the excitation frequency of 2.00 eV of the Ag_{20}-pyridine complex with surface and vertex binding configurations are plotted versus the applied potentials in Fig.4(b). The surface and vertex configurations are colored blue and red, respectively. The solid and dashed lines correspond to the total and chemical enhancements, respectively. The effect of applied potentials on electronic structures was modeled via an orbital energy shift approximation (OESA).[225,226,293] OESA assumes that the INDO parameters

corresponding to the Ag s, p, and d atomic orbital energies are shifted by a value corresponding to the applied potential. In this example, the studied potentials ranged from 0.0 to 2.0 V. Fig.4(b) shows that for both configurations, the electromagnetic enhancements were almost constant in the studied potential range. The surface complex had a steep increase of the chemical enhancement at more negative potentials, but this increase was largely absent in the vertex complex. This observation was explained by the excited state energies of the surface and vertex complexes shown in Fig.4(c) and (d). The solid red, dotted red, and gray lines correspond to the states with significant, minor, and no CT character respectively. Fig.4 (c) and (d) show that, in general, the energies of the CT states were significantly decreased by increasing the potential, and the surface complex had lower CT states than the vertex complex at each potential. At the 2.0 V potential, several states with significant CT character of the surface complex had low enough energies to be excited and provided large contributions to the enhancement. In contrast, the CT states of the vertex complex had higher energies and did not allow for significant CT resonance enhancements at 2.00 eV within this range of potentials. Thus, the potential dependence of the enhancements was mainly explained by the shift of the CT states, and the surface configuration led to CT states with lower energies than the vertex configuration.

The potential dependence of the enhancement can also originate from potential-dependent geometric changes, not only electronic structure changes.[229,294] To investigate the importance of the two factors, INDO/SCI was applied to study a CO molecule attached to the Ag_{20} cluster under external potentials, and the simulation result was compared with the experimental result.[225] Enhancements of the model system under external potentials with constant geometry as well as geometry re-optimized under the external potentials were decomposed into chemical and electromagnetic contributions by INDO/SCI. The result showed that the potential dependence of the enhancements cannot be explained by geometric changes only and was mainly attributed to the shift of the CT states by the external potentials. Besides the above discussed examples, INDO/SCI has also been applied to explain enhancements of semiconductor substrates and quantum effects in TERS imaging.[155,160,295]

D. ORIGIN OF THE TRANSITION-BASED INTERPRETATION OF CHEMICAL ENHANCEMENTS

The above discussed models all interpret chemical enhancements based on electronic transitions. To discuss the origin of the transition-based interpretation, we can briefly review different levels of theory for Raman scattering. A quantum-field description of Raman scattering can be constructed where the electrons, nuclei, and photons involved in the Raman scattering are all treated quantum mechanically. This quantum-field description of Raman scattering has been applied to study Raman enhancements in junctions and cavities.[296–300] The model complexity can be reduced by approximating photons as classic electromagnetic fields, and the Raman scattering can be solved as a second order perturbation response, which leads to the famous Kramers-Heisenberg-Dirac (KHD) formula.[301,302] The KHD formula shows that transitions between vibronic states contribute collectively to the Raman intensity, and each contribution is determined by the corresponding transition dipole moment and excitation energy. Albrecht further approximated the KHD formula by decomposing the vibronic wavefunctions into electronic and nuclear wavefunctions using the Born-Oppenheimer approximation. HT expansion was introduced where vibronic transition dipole moments were expanded at the ground state equilibrium geometry with respect to vibrations.[303–305] For nonresonant Raman scattering, Albrecht also approximated the energy gaps between the vibronic levels by the energy gaps between electronic levels.[305] Similar approximations were also adopted by Placzek to connect the KHD formula to the classic polarizability theory of Raman scattering.[306–308] Later, the classic polarizability theory of Raman scattering was extended to include both nonresonant and resonant conditions by transforming the KHD formula to the time domain and applying the short time approximation.[254,307,309–315] Therefore, the Raman scattering can be interpreted as the vibrational modulation on the electronic polarizability, and the electronic polarizability can be calculated by summing electronic transitions.

In the discussed models, the unified view of SERS was directly inspired by the Albrecht's model of Raman scattering. In both models, the HT expansion was applied and the energy gaps between vibronic states were approximated by the energy gaps of electronic states. The main change made by Lombardi and Birke was to include the states from the metal. The plasmonic states of the metal was simplified by a complex dielectric function, and the CT states were simplified by the Fermi level. Considering the CT transition in the A term only in the unified view of SERS at the static limit would lead to the enhancement formula by the two-state model. By re-

ducing the transitions in the sum-over-state formula, the two-state model focuses on the lowest CT transition, and explains chemical enhancements by the variance of the CT gap. In the INDO/SCI studies, electronic transitions were summed to calculate electronic polarizabilities, and the Raman spectra were calculated by geometric derivatives of the electronic polarizabilities. The derivatives of both excitation energies and transition dipole moments were implicitly considered. Different INDO parameters were applied to determine whether to include the CT transitions when evaluating the electronic polarizabilities so that the enhancements were decomposed into chemical and electromagnetic contributions.

III. THE CHARGE-BASED INTERPRETATION

A. RAMAN BOND MODEL

SERS enhancements originate from interactions between molecules and metal surfaces. To correctly evaluate enhancements, it is important to incorporate a large number of states of the metal surfaces in electronic structure simulations. Choosing electronic structure simulations to study SERS naturally leads to the transition-based interpretation of SERS enhancements. However, the many intra-metal and CT transitions in the simulations make the transition analysis an impractical task. More importantly, chemical information at the molecule-metal interfaces can be easily blurred in the analysis of many transitions. To simplify the transition analysis, the intra-metal transitions can be simplified by dielectric functions of the metal surfaces, and this choice has been made in the unified view of SERS and QM/MM studies of SERS.[316–338] The CT transitions can also be simplified by considering only the lowest CT transition, and this choice has been made in the two-state model and the unified view of SERS. These models are helpful for developing chemical intuition of SERS enhancements from complex electronic structures of SERS systems. However, these models mainly provide qualitative analysis of enhancements, and parameters in the models make their explanations depend on the fitting quality or presumptions. For example, the two-state model cannot quantitatively explain the vibration dependence of enhancements. Symmetry analysis of transitions and vibrations in the unified view of SERS relies on the presumed symmetry of SERS systems. Such presumption is based on the symmetry of unbound molecules and only works for weakly bonded systems. The transition-based interpretation also appears to be inconvenient when comparing electronic structures of localized and periodic model system.

Mapping transitions between states in localized systems and transitions between bands in periodic systems is inconvenient despite the fact that bands are just groups of closely spaced states.

The transition analysis can be avoided by interpreting chemical enhancements based on charge flows near the molecule-metal interface. Similar ideas have been proposed in the previous CM studies. For example, based on a jellium model, McCall and Platzman explained that SERS enhancements were due to vibrational modulation of the reflectivity at the molecule-metal interface.[339] The Persson group explained chemical enhancements by vibrational modulations of electron densities near the molecule-metal interface.[340,341] In another model the Raman response is partitioned to atomic and bond contributions, named Raman atoms and Raman bonds. The bond contributions are dominant, and therefore the model is named the Raman bond model.[342–344] The idea of decomposing Raman response to fragment contributions has been applied in an orbital-based partitioning before.[345] However, the orbital-based partitioning result was dependent on the choices of the origin and the basis set. In the Raman bond model, the Hirshfeld charge model[346] was applied to avoid the basis set dependence, and the atomic charges were distributed as inter-atomic charge flows[347] to solve the origin dependence.

In the Raman bond model, the polarizability derivative is expressed as

$$\frac{\partial \alpha_{ab}}{\partial Q_k} = \sum_i \frac{\partial\{-\int (\boldsymbol{r}_b - \boldsymbol{R}_{i,b})\delta\rho_{i,a} d\boldsymbol{r}\}}{\partial Q_k} + \sum_{ij,j>i} \frac{\partial\{q_{ij,a}(\boldsymbol{R}_{i,b} - \boldsymbol{R}_{j,b})\}}{\partial Q_k}\,, \tag{7}$$

where a and b are directions in the Cartesian space. α_{ab} is one component in the polarizability tensor. Q_k is a vibrational mode. $\boldsymbol{r}$ and $\boldsymbol{R}$ are electronic and nuclear coordinates, respectively. $\rho_{i,a}$ is the induced atomic charge density of atom i polarized in direction a. $q_{ij,a}$ is the charge flow between atoms i and j polarized in direction a. Although charge flows are not uniquely determined given a set of atomic charges, a stable charge flow pattern can be achieved if long-range charge flows are limited. The first and second terms in the equation are Raman atoms and Raman bonds respectively, which describe the atomic and bond contributions to the polarizability derivative. By adopting the Raman bond model, SERS enhancements can be quantitatively analyzed by dozens of atomic and bond contributions, and the analysis of many transitions is avoided. A visual explanation of enhancements can be achieved by mapping the Raman atoms and bonds to the atoms and bonds of the studied system. Raman atoms and bonds can be visualized as spheres and cylinders, whose volumes and colors represent the magnitudes and phases of the contributions, respectively.

It has been demonstrated that the Raman bond model can be applied to both localized and periodic systems and works consistently for different types of molecule-metal bonds.[342–344] To

demonstrate how the Raman bond model is applied to explain enhancements of localized and periodic systems, a group of CO-Ag systems with or without periodic boundary conditions are discussed. The structures and Raman bond patterns of the CO-Ag systems are shown in Fig.5. The enhancement of CO on a 2×2, 2-layer Ag(111) slab [Fig.5(a)] is about 4. The enhancement of CO on a 2×2, 4-layer Ag(111) slab [Fig.5(b)] is about 3. This comparison shows that increasing the slab thickness does not increase the enhancement. However, adding an adatom to the slab increases the enhancement significantly. The enhancement of CO on a 2×2, 2-layer slab with an adatom [Fig.5(c)] is about 13. This comparison shows that it is more effective to promote enhancements by creating surface roughness than increasing surface thickness. The effect of surface roughness can also be demonstrated in localized CO-Ag systems, where the surface binding configuration [Fig.5(d)] models a flat surface, and the vertex binding configuration [Fig.5(e)] models a rough surface. The enhancement of CO on the surface is about 38, while the enhancement of CO on the vertex is about 1885. The enhancement changes can be explained by the Raman bond patterns. In general, the constructive Raman bonds colored blue distribute near the molecule-metal interface and have dominant magnitudes. The destructive Raman bonds colored red distribute in the slab and have small magnitudes. A common Raman bond pattern is found for the localized and periodic systems such that a cone-shaped network of constructive Raman bonds is formed in the metal, and the chemical enhancement is determined by the Raman bonds distributed near the molecule-metal interface. Fig.5(a) and (b) show that adding the two extra layers of Ag atoms barely changes the Raman bond pattern. The Raman bonds in the added layers are destructive and have negligible magnitudes. The small changes of the Raman bonds can be explained by the small change of the inter-fragment charge flow, which does not help the molecular vibration to more effectively modulate charge flows near the molecule-metal interface. This pattern can be explained by the idea that the vibrational modulation on the charge flows in the added layers is screened by the charge flows in the top layers of the slab. In contrast, Fig.5(a) and (c) show that adding the adatom introduces new constructive Raman bonds between the adatom and the Ag atoms underneath, and the destructive Raman bonds in the metal become weaker. Introducing the adatom leads to a nontrivial increase of the inter-fragment charge flow, which leads to more effective and coherent charge flow modulations across the molecule-metal interface. Fig.5(d) and (e) show that the vertex binding leads to stronger and more coherent Raman bonds across the whole system than the surface binding. The explanation of the surface roughness effect on chemical enhancements for the periodic systems is also valid for the localized systems. The surface roughness modeled by

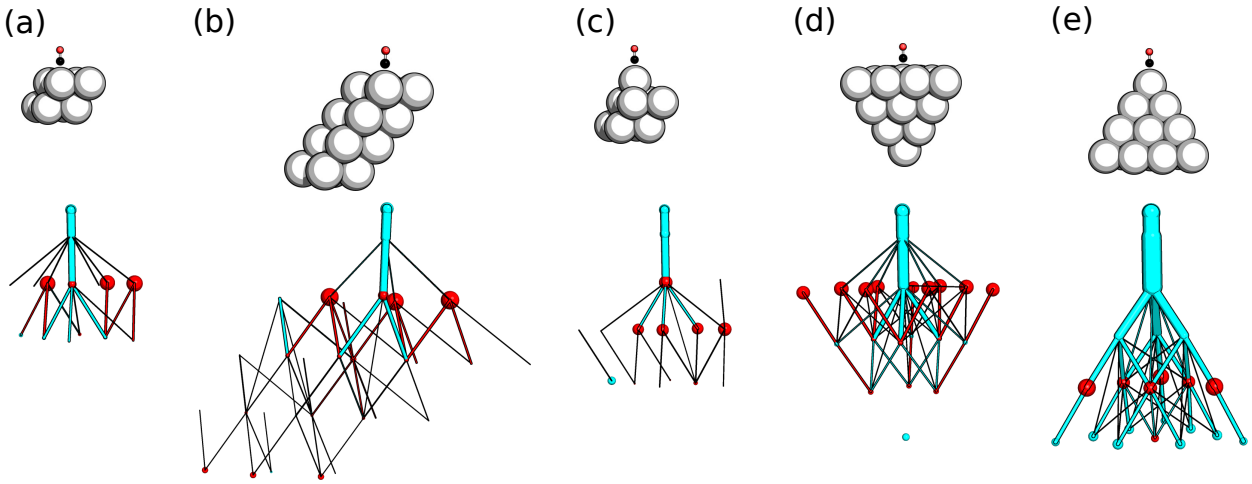

FIG. 5. The Raman bond patterns of CO on a 2×2, 2-layer slab, a 2×2, 4-layer slab, a 2×2, 2-layer slab with an adatom, a surface of a Ag_{20} cluster, a vertex of the Ag_{20} cluster are shown in (a) to (e), respectively. Figure adapted from Ref.[344]. Reproduced from J. Chem. Phys. 157, 184705, 2022, with the permission of AIP Publishing

the vertex binding increases the inter-fragment charge flow. Improving the inter-fragment charge flow connectivity enhances Raman bonds and expands constructive Raman bonds in the metal, which leads to a larger chemical enhancement. It has been shown in EM that surface roughness creates hot spots of EM enhancements where local fields are significantly enhanced. The Raman bond model shows in both periodic and localized systems that surface roughness also creates hot spots of chemical enhancements where the inter-fragment charge flow connectivity is significantly improved. The Raman bond patterns can be simplified as contributions from the molecule, the inter-fragment bond, and the metal by grouping Raman atoms and bonds in the corresponding parts of the system. A quantitative analysis of the inter-fragment charge flows and the three component contributions for the CO-Ag systems is provided in Ref. 344.

The Raman bond model can also visually explain mode-specific enhancements. The enhancements of two ring breathing modes around 1000 cm^{-1} (mode ν_1 and ν_{12}) of pyridine on the Ag surface are interpreted here using the Raman bond model. The vibrational patterns and Raman bond distributions of the selected modes are shown in Fig.6 for a free pyridine molecule and a pyridine-Ag_{20} system. For the free pyridine molecule, the ratio of the Raman intensities of the two ring breathing modes is about 1. Fig.6 (c) and (d) show that the two modes both mainly generate four constructive and two destructive Raman bonds with similar magnitudes, which explains

the similar Raman intensities. The constructive Raman bonds are distributed in the pyridine ring near the N atom for the mode ν_1 while away from the N atom for the mode ν_{12}. The distributions of the Raman bonds are consistent with the atomic motions of the two modes. When the pyridine is adsorbed on the Ag surface, the mode ν_1 is more enhanced than the mode ν_{12}. The ratio of the Raman intensities of the two modes for the pyridine-Ag_{20} system is about 20. Fig.6 (e) and (f) show that the vibrational patterns are not significantly changed due to the adsorption, and the enhancement difference is explained by the Raman bond patterns in Fig.6 (g) and (h). More constructive and stronger Raman bonds are generated at the molecule-metal interface for the mode ν_1 than the mode $_{12}$, which explains the enhancement difference. Compared with the mode ν_{12}, the mode ν_1 involves more N motion and perturbs the N-Ag bond more. Thus, the mode ν_1 more effectively modulates the charge flows at the molecule-metal interface and generate more coherent and strong Raman bonds, which leads to a larger enhancement.

Coupled with the damped response theory, the Raman bond model can also provide a consistent interpretation of enhancements for both non-resonant and resonant conditions. The contributions of the molecule, the inter-fragment bond, and the metal can be mapped to the enhancement contributions of RRS, CT, and EM. The mapping quantifies different enhancement mechanisms based on Raman bond distributions. It is indicated by the mapping that enhancements at any incident frequency are determined by the interference among the coupled mechanisms. The mapping also defines EM in electronic structure simulations as charge flow modulations in the metal. This definition of EM may provide insights for building one holistic theory of SERS which includes CM and EM in a full quantum mechanical theory.

To demonstrate this mapping, enhancements at different incident frequencies of a pyridine-Ag_{20} system are discussed. When a non-zero incident frequency is applied, the polarizability derivative and corresponding contributions from the molecule, the inter-fragment bond, and the metal become complex numbers. The complex quantities can be considered as vectors on the complex plane and projected to the total polarizability derivative. This renders these quantities real and simplifies the analysis. The projections of the total polarizability derivatives (p^{total}), the contributions from the molecule (p^{mol}), the inter-fragment bond (p^{inter}), and the metal (p^{metal}) are plotted versus the incident frequencies for a ring breathing mode of the pyridine-Ag_{20} system in Fig.7(a). The plot shows that the total polarizability derivatives or contributions from any part of the system form a platform in the low frequency range where no resonance is excited. The off-resonance enhancements originate from the ground state chemical interaction between the

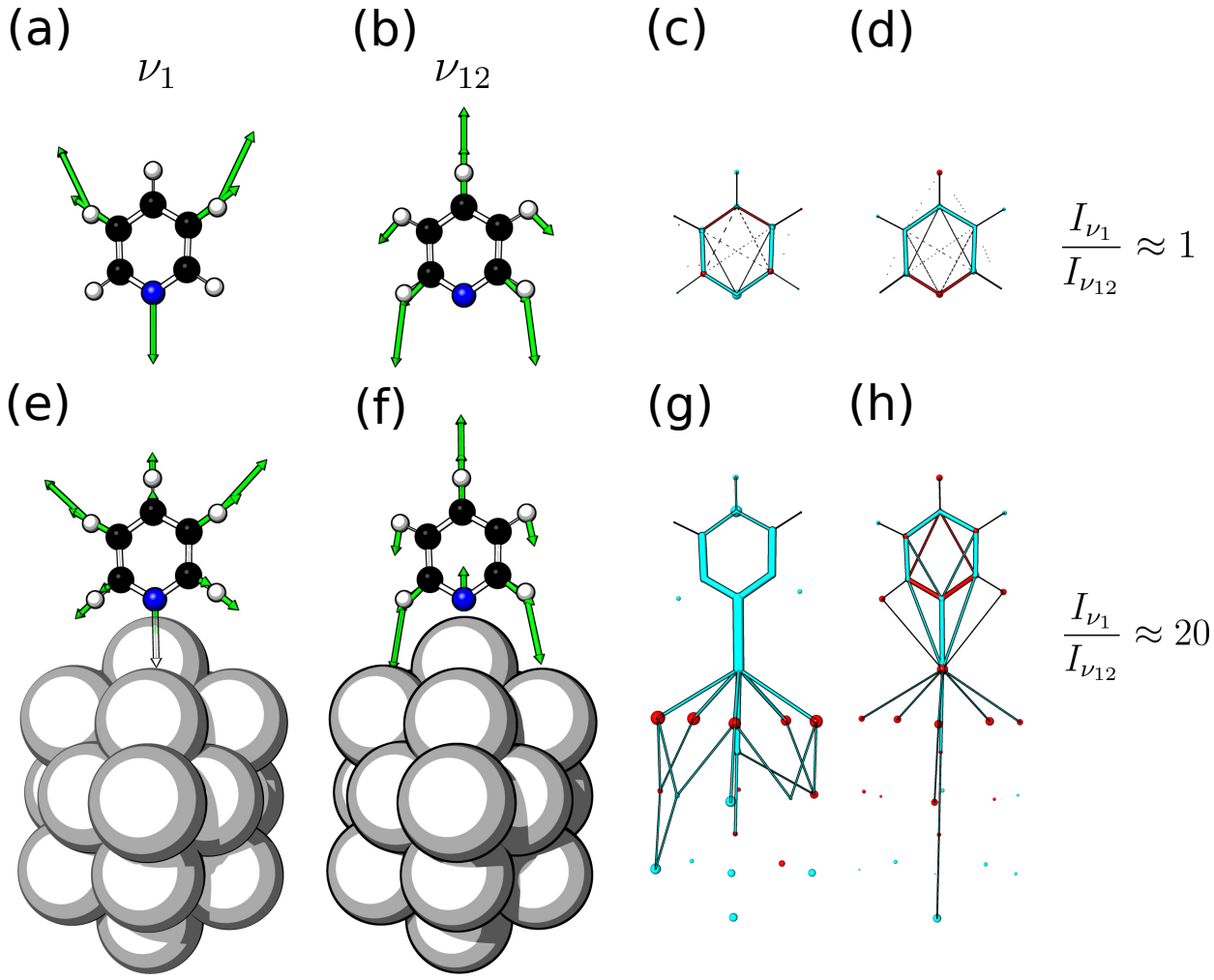

FIG. 6. The vibrational patterns of mode ν_1 and ν_{12} are shown in (a) and (b) for the free pyridine and (e) and (f) for the pyridine-Ag_{20} system. The Raman bond patterns of mode ν_1 and ν_{12} are shown in (c) and (d) for the free pyridine and (g) and (h) for the pyridine-Ag_{20} system. Adapted from Ref.[343] Reproduced from J. Chem. Phys. 152, 024126, 2020, with the permission of AIP Publishing

molecule and the metal and is labeled as CHEM. The first peak occurs at around 2.35 eV, corresponding to the charge-transfer resonance and labeled as CT. At the CT resonance, the contribution of the inter-fragment bond is shown to be dominant. The largest peak occurs at around 3.40 eV, corresponding to the cluster resonance. The peak is labeled as EM because the cluster resonance approximately models the surface plasmon resonance. At the cluster resonance, the metal contribution is shown to be dominant. The last significant peak occurs at 6.20 eV, corresponding to the molecular resonance and labeled as RRS. At the molecular resonance, the molecular contribution is shown to be dominant. The plot shows that the distribution of the dominant Raman bonds

is consistent with the resonant condition. The contributions of the molecule, the inter-fragment bond, and the metal can be applied to quantify the enhancement contributions of the molecular resonance, the CT resonance, and the plasmon resonance.

This mapping can be examined in detail in the Raman bond patterns. The Raman bond patterns of the ring breathing mode at the static limit, the CT resonance, the cluster resonance, and the molecular resonance are shown in Fig.7(b) to (e), respectively. In the plots, the Raman atoms and bonds are also considered as vectors on the complex plane. The phases and lengths of the Raman atoms and bonds are represented by colors and volumes of the spheres and cylinders. Fig.7(b) shows that at the static limit, the Raman bonds mainly distribute in the molecule, and about 93% of the polarizability derivative is contributed by the molecule. The charge flows in the metal are not effectively modulated by the molecular vibration. Fig.7(c) to (e) show that, compared with the static limit, the Raman bonds across the system are enhanced if any resonance is excited. The dominant Raman bonds in Fig.7(c) to (e) highlighted in the orange boxes distribute in the inter-fragment bond, the metal, and the molecule. The dominant Raman bonds in Fig.7(c) to (e) contribute about 60%, 100%, and 61% of the total polarizability derivative, respectively. The distributions of the Raman bonds are consistent with the spatial distributions of the resonance. It is worth noting that at any resonance, the Raman bonds distribute across the whole system as the resonance is not perfectly localized. In the previous study, we have shown that when the inter-fragment charge flow was increased, the spacial distributions of the resonance or the Raman bonds were more delocalized.[342]

In the pyridine-Ag_{20} example, the Raman bonds in the metal are mapped to the enhancement contribution of the surface plasmon resonance. In EM, the enhancement contribution of the surface plasmon resonance is modeled as the enhanced local field amplifying the polarizability derivative of the molecule. To connect the Raman bonds in the metal and the enhanced local field, we can apply the Silberstein equation to treat the molecule and the metal as two polarizable dipoles.[74,91,348] The model is schematically illustrated in Fig.8 where the molecular and metal (nanoparticle) polarizabilities are α^{M} and α^{NP}, and the distance between the molecule and the metal is R. In the model, the chemical bonding between the molecule and the metal is not included, and thus the polarizability of the inter-fragment bond is not considered. The total polarizability for the system parallel to the molecule–metal axis is

$$\alpha_{\parallel}^{\mathrm{total}} = \frac{\alpha^{\mathrm{M}} + \alpha^{\mathrm{NP}} + 4\alpha^{\mathrm{M}}\alpha^{\mathrm{NP}}/R^3}{1 - 4\alpha^{\mathrm{M}}\alpha^{\mathrm{NP}}/R^6} \,. \tag{8}$$

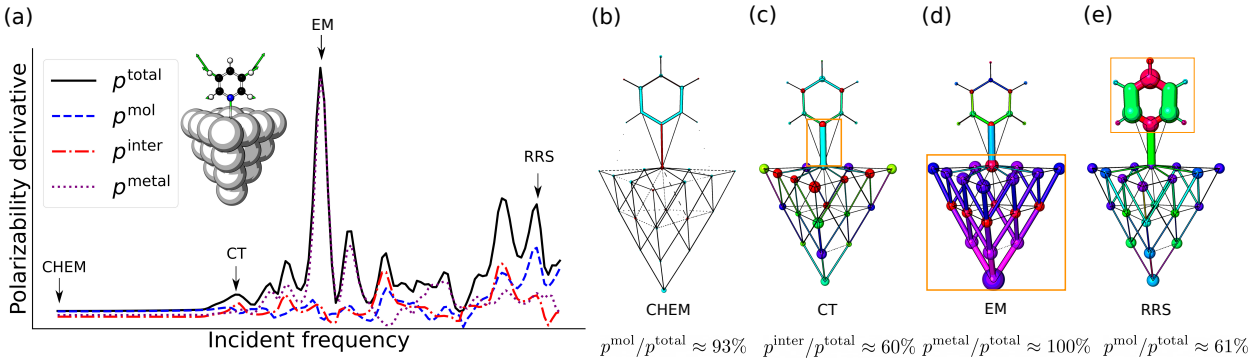

FIG. 7. The total polarizability derivatives (p^{total}) are plotted versus the incident frequencies for a ring breathing mode of a pyridine-Ag_{20} system in (a). At each incident frequency, the total polarizability derivative is partitioned to the contributions of the molecule (p^{mol}), the inter-fragment bond (p^{inter}), and the metal (p^{metal}). The Raman bond patterns of the ring breathing mode of the pyridine-Ag_{20} system at the static limit, the charge transfer resonance, the cluster resonance, and the molecular resonance are shown in (b) to (e). Adapted from Ref.[342]. Reproduced from J. Chem. Phys. 153, 224704, 2020 with the permission of AIP Publishing

Accordingly, the polarizability derivative of the system is

$$\frac{\partial \alpha_{\parallel}^{\text{total}}}{\partial Q_k} = \frac{\partial \alpha^{\text{M}}}{\partial Q_k} \frac{(1+2\alpha^{\text{NP}}/R^3)^2}{(1-4\alpha^{\text{NP}}\alpha^{\text{M}}/R^6)^2} \,. \tag{9}$$

The factor scaling the molecular polarizability derivative can be considered as the square of the local field enhancement.

Alternatively, the total polarizability can be partitioned based on the relative volumes of the molecule and the metal as

$$\alpha_{\parallel}^{\text{total}} \approx \alpha^{\text{M}} + \alpha^{\text{NP}} + (4\alpha^{\text{M}}\alpha^{\text{NP}}/R^3)\left(\frac{V^{\text{M}}}{V^{\text{M}}+V^{\text{NP}}} + \frac{V^{\text{NP}}}{V^{\text{M}}+V^{\text{NP}}}\right) , \tag{10}$$

where V^{M} and V^{NP} are the volumes of the molecule and the metal. Here the image field effect is neglected, and $4\alpha^{\text{M}}\alpha^{\text{NP}}/R^3$ describes the electromagnetic interaction between the molecule and the metal.

The partitioned interaction term can lead to effective polarizabilities of the molecule and the metal:

$$\begin{aligned} \alpha_{\text{eff}}^{\text{M}} &= \alpha^{\text{M}} + (4\alpha^{\text{M}}\alpha^{\text{NP}}/R^3)\frac{V^{\text{M}}}{V^{\text{M}}+V^{\text{NP}}} \,, \\ \alpha_{\text{eff}}^{\text{NP}} &= \alpha^{\text{NP}} + (4\alpha^{\text{M}}\alpha^{\text{NP}}/R^3)\frac{V^{\text{NP}}}{V^{\text{M}}+V^{\text{NP}}} \,. \end{aligned} \tag{11}$$

Accordingly, the total polarizability derivative can be written as

$$\frac{\partial \alpha_{\parallel}^{\text{total}}}{\partial Q_k} \approx \frac{\partial \alpha_{\text{eff}}^{\text{M}}}{\partial Q_k} + \frac{\partial \alpha_{\text{eff}}^{\text{NP}}}{\partial Q_k} \,. \tag{12}$$

Such volume-based partitioning is consistent with the Hirshfeld partitioning adopted in the Raman bond model. The effective polarizability derivatives of the molecule and the metal can be mapped to the Raman bonds in the molecule and the metal, respectively. Because the volume of the metal is significantly larger than the molecule, this volume-based partitioning will assign most of the electromagnetic interaction to the metal. At the surface plasmon resonance, the derivative of the effective polarizability of the metal will dominate and determine the enhancement. The derivative of the effective polarizability of the metal corresponds to the Raman bonds in the metal shown on the right side of Fig.8. It should be noted that the Raman bonds in the metal can also be induced by charge transfer between the molecule and the metal. Thus, the connection between the Raman bonds in the metal and the enhanced local field can only be established when the charge transfer is limited. When the charge transfer is significant, the local field can be quenched due to the screening effect of the charge transfer between the molecule and the metal surface, and this idea is demonstrated in a recent TERS study.[349] However, the quenching of the local field due to the molecule-metal charge transfer does not necessarily decrease the overall SERS enhancement. In a previous study, we have showed that the overall enhancement can be almost unchanged when the molecule-metal charge transfer is increased because the increased chemical enhancement can compensate the decreased EM enhancement.[342] It is also worth mentioning that quenching of the SERS response can have different meanings in different contexts. In the recent TERS study,[349] the quenching of the SERS response is discussed when comparing a tip-molecule system on a NaCl surface and a tip-molecule system on an Ag surface. The quenching of the SERS response can also be discussed when comparing a molecule-metal system and the isolated molecule, where the enhancement would be less than 1.[223]

In the above discussed examples, it has been shown that when the inter-fragment charge flow is increased, charge flows across the system can be modulated more effectively and coherently by the molecular vibration, which leads to a larger enhancement. A linear correlation between the enhancements and the inter-fragment charge flows to the fourth power for both localized and periodic systems can be found. The correlation is demonstrated by applying chemical substitutions, electric fields, and charges to tune the enhancements of a C-H bending mode of the pyridine-Ag_{20} system, shown in Fig.9(a). The enhancements are shown to be correlated to the inter-fragment

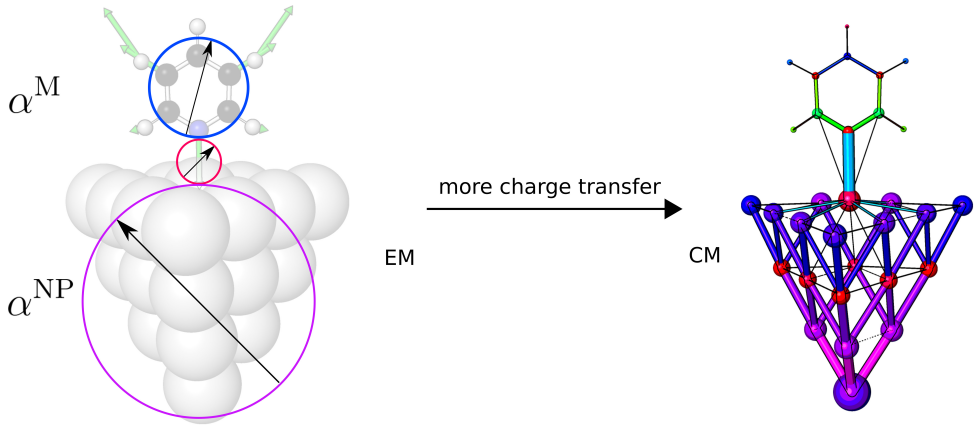

FIG. 8. A diagram of illustrating the Silberstein equation[348] is shown on the left side. The Raman bond pattern at the cluster resonance is shown on the right side.

charge flows to the fourth power. It should be noted that the inter-fragment charge flow is induced by the incident light and does not necessarily scale with the ground state charge transfer. In the pyridine-Ag_{20} system, the enhancement is found to increase by introducing electron pulling groups, positive charges, and electric fields pointing from the molecule to the metal. These tuning factors increase the induced charge transfer but decrease the ground state charge transfer. The correlation between the enhancement and the inter-fragment charge flow is also found in systems with CO on different Ag clusters or slabs, shown in Fig.9(b) and (c). For the localized CO-Ag systems, the enhancement is found to increase if surface roughness is created and the cluster is elongated along the polarization direction. For the periodic CO-Ag system, the enhancement is found to increase if surface roughness is created and a low surface coverage is adopted.

B. CONNECTION BETWEEN THE INTERPRETATIONS

Both the transition-based and charge-based interpretations of chemical enhancements are rooted in the classic polarizability theory of Raman scattering, where Raman scattering is explained as geometric derivatives of electronic polarizabilities. The difference is that the transition-based interpretation considers the electronic polarizability as a sum of electronic transitions, while the charge-based interpretation considers the electronic polarizability as charge flows between atoms. Different treatments of the electronic polarizability lead to different interpretations of enhancements.

The connection between these two interpretations is provided by the correlation between the

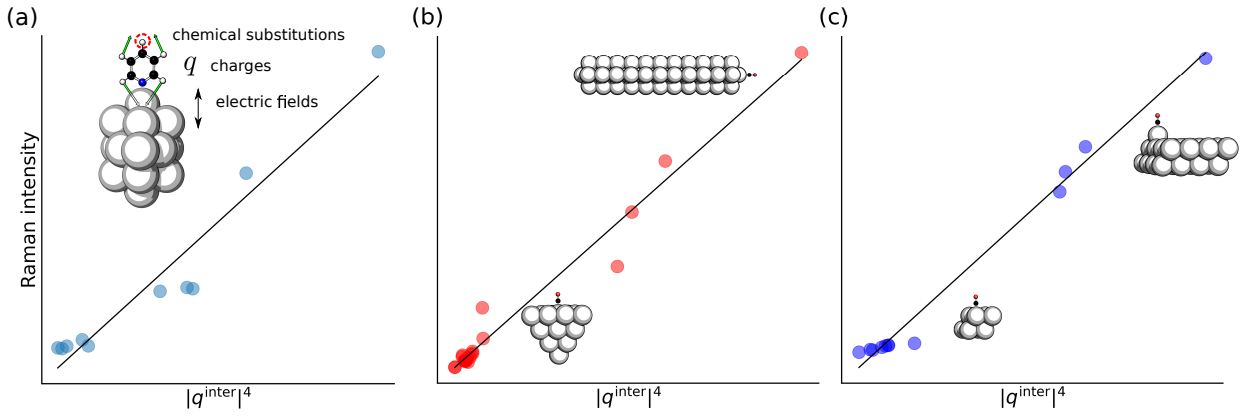

FIG. 9. The Raman intensities of a C-H bending mode of pyridine-Ag_{20} systems are plotted versus the inter-fragment charge flows to the fourth power in (a). The Raman intensities of the C-O stretching mode are plotted versus the inter-fragment charge flows to the fourth power for CO on different Ag clusters in (b). The Raman intensities of the C-O stretching mode are plotted versus the inter-fragment charge flows to the fourth power for CO on different Ag slabs in (c).

enhancements and the inter-fragment charge flows found by the Raman bond model. Such correlation resembles the conclusion of the two-state model that the chemical enhancements are inversely proportional to the CT excitation energies to the fourth power. Since decreasing the CT excitation energy would increase the inter-fragment charge flow, we can expect that the inter-fragment charge flow is inversely proportional to the CT excitation energy. Then, the conclusion of the two-state model would lead to the correlation found by the Raman bond model. The transition based interpretation shows that a larger chemical enhancement can be achieved by decreasing the CT gap. Accordingly, the charge-based interpretation shows that a larger chemical enhancement can be achieved by increasing the inter-fragment charge flow. The connection between the two interpretations is that decreasing the CT energy gap leads to more dynamic polarization at the molecule-metal interface and increases the inter-fragment charge flow.

IV. CONCLUSION

An overview is given for models explaining SERS enhancements based on electronic structure simulations. The models provide a transition-based and a charge-based interpretations of SERS enhancements. In the transition-based interpretation, Raman scattering is explained as vibrational modulations on electronic transitions, and SERS enhancements arise from molecular transitions

with decreased energy gaps and new CT transitions. The transition-based interpretation can be directly applied to analyze results of electronic structure simulations, and provide clear explanations of enhancements when specific transitions can be identified as dominant contributions. The transition-based interpretation also has inspired methods to tune orbital mixing between molecules and metal to decompose enhancements.

In the charge-based interpretation, Raman scattering is explained as vibrational modulations on interatomic charge flows, and SERS enhancements are explained by charge flow modulations near the molecule-metal interfaces. To discuss the charge-based interpretation, a recently developed Raman bond model is introduced. The charge-based interpretation can be easily visualized and connected to chemical intuition by overlapping charge flow networks with bonding networks of SERS systems A unified and quantitative explanation of enhancements for localized and periodic model systems can be obtained by the charge-based interpretation. The enhancement contributions of molecular resonance, CT resonance, and plasmon resonance can be quantified by the charge flow modulations in the molecule, the inter-fragment bond, and the metal. The polarization near the molecule-metal interfaces is emphasized in both interpretations. The interfacial polarization is characterized by the CT gaps in the transition-based interpretation while by the inter-fragment charge flows in the charge-based interpretations.

ACKNOWLEDGMENTS

The authors gratefully acknowledge financial support from National Science Foundation Grant CHE-2106151.

REFERENCES

[1]M. Fleischmann, P. Hendra, and A. McQuillan, "Raman spectra of pyridine adsorbed at a silver electrode," Chem. Phys. Lett. **26**, 163 – 166 (1974).

[2]D. L. Jeanmaire and R. P. Van Duyne, "Surface raman spectroelectrochemistry: Part i. heterocyclic, aromatic, and aliphatic amines adsorbed on the anodized silver electrode," J. Electroanal. Chem. Interfacial Electrochem. **84**, 1–20 (1977).

[3]M. G. Albrecht and J. A. Creighton, "Anomalously intense raman spectra of pyridine at a silver electrode," J. Am. Chem. Soc. **99**, 5215–5217 (1977).

[4]A. Campion, "Raman spectroscopy of molecules adsorbed on solid surfaces," Ann. Rev. Phys. Chem. **36**, 549–572 (1985).

[5]L. A. Sanchez, J. R. Lombardi, and R. L. Birke, "Surface enhanced raman scattering of ammonia," Chem. Phys. Lett. **108**, 45–50 (1984).

[6]B. Pettinger, K. Krischer, and G. Ertl, "Giant raman scattering cross section for an adsorbed dye at ag colloids associated with low em field enhancement," Chem. Phys. Lett. **151**, 151–155 (1988).

[7]P. Hildebrandt and M. Stockburger, "Surface-enhanced resonance Raman spectroscopy of Rhodamine 6G adsorbed on colloidal silver," J. Phys. Chem. **88**, 5935–5944 (1984).

[8]W.-H. Yang, J. Hulteen, G. C. Schatz, and R. P. Van Duyne, "A surface-enhanced hyper-raman and surface-enhanced raman scattering study of trans-1,2-bis(4-pyridyl)ethylene adsorbed onto silver film over nanosphere electrodes. vibrational assignments: Experiment and theory," J. Chem. Phys. **104**, 4313 (1996).

[9]Y. Fang, N.-H. Seong, and D. D. Dlott, "Measurement of the distribution of site enhancements in surface-enhanced Raman scattering," Science **321**, 388–392 (2008).

[10]K. Imura, H. Okamoto, M. K. Hossain, and M. Kitajima, "Visualization of localized intense optical fields in single gold-nanoparticle assemblies and ultrasensitive raman active sites," Nano Lett. **6**, 2173–2176 (2006).

[11]T. A. Laurence, G. B. Braun, N. O. Reich, and M. Moskovits, "Robust sers enhancement factor statistics using rotational correlation spectroscopy," Nano Lett. **12**, 2912–2917 (2012).

[12]S. Yang, X. Dai, B. B. Stogin, and T.-S. Wong, "Ultrasensitive surface-enhanced raman scattering detection in common fluids," Proc. Natl. Acad. Sci. USA **113**, 268–273 (2016).

[13]K.-i. Yoshida, T. Itoh, H. Tamaru, V. Biju, M. Ishikawa, and Y. Ozaki, "Quantitative evaluation of electromagnetic enhancement in surface-enhanced resonance raman scattering from plasmonic properties and morphologies of individual ag nanostructures," Phys. Rev. B **81**, 115406 (2010).

[14]R. Alvarez-Puebla, L. M. Liz-Marzán, and F. J. García de Abajo, "Light concentration at the nanometer scale," J. Phys. Chem. Lett. **1**, 2428–2434 (2010).

[15]D.-K. Lim, K.-S. Jeon, H. M. Kim, J.-M. Nam, and Y. D. Suh, "Nanogap-engineerable raman-active nanodumbbells for single-molecule detection," Nat. Mater. **9**, 60–67 (2010).

[16]D.-K. Lim, K.-S. Jeon, J.-H. Hwang, H. Kim, S. Kwon, Y. D. Suh, and J.-M. Nam, "Highly uniform and reproducible surface-enhanced raman scattering from dna-tailorable nanoparticles

with 1-nm interior gap," Nat. Nanotechnol. **6**, 452–460 (2011).

[17]K. L. Wustholz, A.-I. Henry, J. M. McMahon, R. G. Freeman, N. Valley, M. E. Piotti, M. J. Natan, G. C. Schatz, and R. P. V. Duyne, "Structure-activity relationships in gold nanoparticle dimers and trimers for surface-enhanced raman spectroscopy," J. Am. Chem. Soc. **132**, 10903–10910 (2010).

[18]H. Wang, C. S. Levin, and N. J. Halas, "Nanosphere arrays with controlled sub-10-nm gaps as surface-enhanced raman spectroscopy substrates," J. Am. Chem. Soc. **127**, 14992–14993 (2005).

[19]W. Li, P. H. C. Camargo, X. Lu, and Y. Xia, "Dimers of silver nanospheres: Facile synthesis and their use as hot spots for surface-enhanced raman scattering," Nano Lett. **9**, 485–490 (2009).

[20]K. Kneipp, Y. Wang, H. Kneipp, L. T. Perelman, I. Itzkan, R. R. Dasari, and M. S. Feld, "Single molecule detection using surface-enhanced Raman scattering (SERS)," Phys. Rev. Lett. **78**, 1667–1670 (1997).

[21]H. Xu, E. J. Bjerneld, M. Käll, and L. Börjesson, "Spectroscopy of single hemoglobin molecules by surface enhanced Raman scattering," Phys. Rev. Lett. **83**, 4357–4360 (1999).

[22]K. Kneipp, H. Kneipp, V. B. Kartha, R. Manoharan, G. Deinum, I. Itzkan, R. R. Dasari, and M. S. Feld, "Detection and identification of a single dna base molecule using surface-enhanced raman scattering (sers)," Phys. Rev. E **57**, R6281–R6284 (1998).

[23]S. M. Nie and S. R. Emory, "Probing single molecules and single nanoparticles by surface-enhanced Raman scattering," Science **275**, 1102–1106 (1997).

[24]A. B. Zrimsek, N. L. Wong, and R. P. Van Duyne, "Single molecule surface-enhanced raman spectroscopy: A critical analysis of the bianalyte versus isotopologue proof," J. Phys. Chem. C **120**, 5133–5142 (2016).

[25]Jiang, K. Bosnick, M. Maillard, and L. Brus, "Single molecule raman spectroscopy at the junctions of large ag nanocrystals," J. Phys. Chem. B **107**, 9964–9972 (2003).

[26]A. M. Michaels, M. Nirmal, and L. E. Brus, "Surface enhanced Raman spectroscopy of individual rhodamine 6G molecules on large Ag nanocrystals," J. Am. Chem. Soc. **121**, 9932–9939 (1999).

[27]T. A. Laurence, G. Braun, C. Talley, A. Schwartzberg, M. Moskovits, N. Reich, and T. Huser, "Rapid, solution-based characterization of optimized sers nanoparticle substrates," J. Am. Chem. Soc. **131**, 162–169 (2009).

[28]J. A. Dieringer, K. L. Wustholz, D. J. Masiello, J. P. Camden, S. L. Kleinman, G. C. Schatz,

and R. P. Van Duyne, "Surface-enhanced Raman excitation spectroscopy of a single rhodamine 6G molecule," J. Am. Chem. Soc. **131**, 849–854 (2009).

[29]J. Chen, W. Ding, Z. Luo, B. H. Loo, and J. Yao, "Probing single molecules and molecular aggregates: Raman spectroscopic advances," J. Raman Spectrosc. **47**, 623–635 (2016).

[30]F. Benz, M. K. Schmidt, A. Dreismann, R. Chikkaraddy, Y. Zhang, A. Demetriadou, C. Carnegie, H. Ohadi, B. de Nijs, R. Esteban, J. Aizpurua, and J. J. Baumberg, "Single-molecule optomechanics in "picocavities"," Science **354**, 726–729 (2016).

[31]N. P. W. Pieczonka and R. F. Aroca, "Single molecule analysis by surfaced-enhanced raman scattering," Chem. Soc. Rev. **37**, 946–954 (2008).

[32]A. B. Zrimsek, N. Chiang, M. Mattei, S. Zaleski, M. O. McAnally, C. T. Chapman, A.-I. Henry, G. C. Schatz, and R. P. Van Duyne, "Single-molecule chemistry with surface- and tip-enhanced raman spectroscopy," Chem. Rev. **117**, 7583–7613 (2016).

[33]E. C. Le Ru and P. G. Etchegoin, "Single-molecule surface-enhanced raman spectroscopy," Ann. Rev. Phys. Chem. **63**, 65–87 (2012).

[34]H.-K. Choi, K. S. Lee, H.-H. Shin, J.-J. Koo, G. J. Yeon, and Z. H. Kim, "Single-molecule surface-enhanced raman scattering as a probe of single-molecule surface reactions: Promises and current challenges," Acc. Chem. Res. **52**, 3008–3017 (2019).

[35]S. Schlücker, "Surface-enhanced raman spectroscopy: Concepts and chemical applications," Angew. Chem., Int. Edit. **53**, 4756–4795 (2014).

[36]J. Langer, D. Jimenez de Aberasturi, J. Aizpurua, R. A. Alvarez-Puebla, B. Auguié, J. J. Baumberg, G. C. Bazan, S. E. J. Bell, A. Boisen, A. G. Brolo, J. Choo, D. Cialla-May, V. Deckert, L. Fabris, K. Faulds, F. J. García de Abajo, R. Goodacre, D. Graham, A. J. Haes, C. L. Haynes, C. Huck, T. Itoh, M. Käll, J. Kneipp, N. A. Kotov, H. Kuang, E. C. Le Ru, H. K. Lee, J.-F. Li, X. Y. Ling, S. A. Maier, T. Mayerhöfer, M. Moskovits, K. Murakoshi, J.-M. Nam, S. Nie, Y. Ozaki, I. Pastoriza-Santos, J. Perez-Juste, J. Popp, A. Pucci, S. Reich, B. Ren, G. C. Schatz, T. Shegai, S. Schlücker, L.-L. Tay, K. G. Thomas, Z.-Q. Tian, R. P. Van Duyne, T. Vo-Dinh, Y. Wang, K. A. Willets, C. Xu, H. Xu, Y. Xu, Y. S. Yamamoto, B. Zhao, and L. M. Liz-Marzán, "Present and future of surface-enhanced raman scattering," ACS Nano **14**, 28–117 (2020).

[37]P. L. Stiles, J. A. Dieringer, N. C. Shah, and R. P. Van Duyne, "Surface-enhanced raman spectroscopy," Annu. Rev. Anal. Chem. **1**, 601–626 (2008).

[38]S. E. J. Bell and N. M. S. Sirimuthu, "Quantitative surface-enhanced Raman spectroscopy," Chem. Soc. Rev. **37**, 1012–1024 (2008).

[39]W. Xiang, H. Sheng-Chao, H. Shu, Y. Sen, and R. Bin, "Fundamental understanding and applications of plasmon-enhanced raman spectroscopy," Nat. Rev. Phys. **2**, 253–271 (2020).

[40]A. I. Pérez-Jiménez, D. Lyu, Z. Lu, G. Liu, and B. Ren, "Surface-enhanced raman spectroscopy: benefits, trade-offs and future developments," Chem. Sci. **11**, 4563–4577 (2020).

[41]R. Gordon, D. Sinton, K. L. Kavanagh, and A. G. Brolo, "A new generation of sensors based on extraordinary optical transmission," Acc. Chem. Res. **41**, 1049–1057 (2008).

[42]C. L. Haynes, A. D. McFarland, and R. P. Van Duyne, "Surface-enhanced raman spectroscopy," Anal. Chem. **77**, 338A–346A (2005).

[43]S. H. Yazdi and I. M. White, "Optofluidic surface enhanced raman spectroscopy microsystem for sensitive and repeatable on-site detection of chemical contaminants," Anal. Chem. **84**, 7992–7998 (2012).

[44]H.-L. Liu, J. Cao, S. Hanif, C. Yuan, J. Pang, R. Levicky, X.-H. Xia, and K. Wang, "Size-controllable gold nanopores with high sers activity," Anal. Chem. **89**, 10407–10413 (2017).

[45]L. Wonkyoung, K. Byoung-Hoon, Y. Hyunwoo, P. Moonseong, K. J. Hyun, C. Taerin, J. Yong, K. B. Kyu, and J. Ki-Hun, "Spread spectrum sers allows label-free detection of attomolar neurotransmitters," Nat Commun. **12**, 159 (2021).

[46]J. N. Anker, W. P. Hall, O. Lyandres, N. C. Shah, J. Zhao, and R. P. Van Duyne, "Biosensing with plasmonic nanosensors," Nat. Mater. **7**, 442–453 (2008).

[47]Y. C. Cao, R. Jin, and C. A. Mirkin, "Nanoparticles with Raman spectroscopic fingerprints for DNA and RNA detection." Science **297**, 1536–1540 (2002).

[48]P. K. Jain, X. Huang, I. H. El-Sayed, and M. A. El-Sayed, "Noble metals on the nanoscale: Optical and photothermal properties and some applications in imaging, sensing, biology, and medicine," Acc. Chem. Res. **41**, 1578–1586 (2008).

[49]Y. Wang, B. Yan, and L. Chen, "Sers tags: Novel optical nanoprobes for bioanalysis," Chem. Rev. **113**, 1391–1428 (2013).

[50]C. Zong, M. Xu, L.-J. Xu, T. Wei, X. Ma, X.-S. Zheng, R. Hu, and B. Ren, "Surface-enhanced raman spectroscopy for bioanalysis: Reliability and challenges," Chem. Rev. **118**, 4946–4980 (2018).

[51]Z. Wang, S. Zong, L. Wu, D. Zhu, and Y. Cui, "Sers-activated platforms for immunoassay: Probes, encoding methods, and applications," Chem. Rev. **117**, 7910–7963 (2017).

[52]M. Vendrell, K. K. Maiti, K. Dhaliwal, and Y.-T. Chang, "Surface-enhanced raman scattering in cancer detection and imaging," Trends in Biotechnology **31**, 249–257 (2013).

[53]A. M. Shrivastav, U. Cvelbar, and I. Abdulhalim, "A comprehensive review on plasmonic-based biosensors used in viral diagnostics," Commun. Biol. **4**, 70 (2021).

[54]A. Sujith, T. Itoh, H. Abe, A. A. Anas, K. Yoshida, V. Biju, and M. Ishikawa, "Surface enhanced raman scattering analyses of individual silver nanoaggregates on living single yeast cell wall," Appl. Phys. Lett. **92**, 103901 (2008).

[55]M. J. Tan, Z.-Y. Hong, M.-H. Chang, C.-C. Liu, H.-F. Cheng, X. J. Loh, C.-H. Chen, C.-D. Liao, and K. V. Kong, "Metal carbonyl-gold nanoparticle conjugates for highly sensitive sers detection of organophosphorus pesticides," Biosens. Bioelectron. **96**, 167–172 (2017).

[56]W. Kim, S. H. Lee, Y. J. Ahn, S. H. Lee, J. Ryu, S. K. Choi, and S. Choi, "A label-free cellulose sers biosensor chip with improvement of nanoparticle-enhanced lspr effects for early diagnosis of subarachnoid hemorrhage-induced complications," Biosens. Bioelectron. **111**, 59–65 (2018).

[57]B. Sharma, R. R. Frontiera, A.-I. Henry, E. Ringe, and R. P. Van Duyne, "Sers: Materials, applications, and the future," Mater. Today **15**, 16–25 (2012).

[58]S.-Y. Ding, J. Yi, J.-F. Li, B. Ren, D.-Y. Wu, R. Panneerselvam, and Z.-Q. Tian, "Nanostructure-based plasmon-enhanced raman spectroscopy for surface analysis of materials," Nat. Rev. Mater. **1**, 16021 (2016).

[59]Z.-Q. Tian and B. Ren, "Adsorption and reaction at electrochemical interfaces as probed by surface-enhanced raman spectroscopy," Ann. Rev. Phys. Chem. **55**, 197–229 (2004).

[60]B. Dong, Y. Fang, X. Chen, H. Xu, and M. Sun, "Substrate-, wavelength-, and time-dependent plasmon-assisted surface catalysis reaction of 4-nitrobenzenethiol dimerizing to p,p′-dimercaptoazobenzene on au, ag, and cu films," Langmuir **27**, 10677–10682 (2011).

[61]V. Joseph, C. Engelbrekt, J. Zhang, U. Gernert, J. Ulstrup, and J. Kneipp, "Characterizing the kinetics of nanoparticle-catalyzed reactions by surface-enhanced raman scattering," Angewandte Chemie International Edition **51**, 7592–7596 (2012).

[62]M. Sun and H. Xu, "A novel application of plasmonics: Plasmon-driven surface-catalyzed reactions," Small **8**, 2777–2786 (2012).

[63]T. Itoh, K. Hashimoto, V. Biju, M. Ishikawa, B. R. Wood, and Y. Ozaki, "Elucidation of interaction between metal-free tetraphenylporphine and surface ag atoms through temporal fluctuation of surface-enhanced resonance raman scattering and background-light emission," J. Phys. Chem. B **110**, 9579–9585 (2006).

[64]E. Cortés, P. G. Etchegoin, E. C. Le Ru, A. Fainstein, M. E. Vela, and R. C. Salvarezza, "Monitoring the electrochemistry of single molecules by surface-enhanced raman spectroscopy," J.

Am. Chem. Soc. **132**, 18034–18037 (2010).

[65]Y. F. Huang, H. P. Zhu, G. K. Liu, D. Y. Wu, B. Ren, and Z. Q. Tian, "When the signal is not from the original molecule to be detected: Chemical transformation of para-aminothiophenol on ag during the sers measurement," J. Am. Chem. Soc. **132**, 9244–9246 (2010).

[66]C. Jing and Y. Fang, "Experimental (SERS) and theoretical (DFT) studies on the adsorption behaviors of l-cysteine on gold/silver nanoparticles," Chem. Phys. **332**, 27–32 (2007).

[67]P. Aravind and H. Metiu, "The effects of the interaction between resonances in the electromagnetic response of a sphere-plane structure; applications to surface enhanced spectroscopy," Surf. Sci. **124**, 506–528 (1983).

[68]M. Moskovits, "Surface roughness and the enhanced intensity of raman scattering by molecules adsorbed on metals," J. Chem. Phys. **69**, 4159–4161 (1978).

[69]G. C. Schatz, "Theoretical studies of surface enhanced raman scattering," Acc. Chem. Res. **17**, 370–376 (1984).

[70]M. Moskovits, "Enhanced raman scattering by molecules adsorbed on electrodes–a theoretical model," Solid State Commun. **32**, 59–62 (1979).

[71]M. Moskovits, "Surface-enhanced spectroscopy," Rev. Mod. Phys. **57**, 783–826 (1985).

[72]J. C. Tsang, J. R. Kirtley, and J. A. Bradley, "Surface-enhanced raman spectroscopy and surface plasmons," Phys. Rev. Lett. **43**, 772–775 (1979).

[73]M. Kerker, D.-S. Wang, and H. Chew, "Surface enhanced raman scattering (sers) by molecules adsorbed at spherical particles: Errata," Appl. Opt. **19**, 4159–4174 (1980).

[74]J. Gersten and A. Nitzan, "Electromagnetic theory of enhanced Raman scattering by molecules adsorbed on rough surfaces," J. Chem. Phys. **73**, 3023–3037 (1980).

[75]P. Aravind and H. Metiu, "The enhancement of raman and fluorescent intensity by small surface roughness. changes in dipole emission," Chem. Phys. Lett. **74**, 301 – 305 (1980).

[76]P. Aravind, A. Nitzan, and H. Metiu, "The interaction between electromagnetic resonances and its role in spectroscopic studies of molecules adsorbed on colloidal particles or metal spheres," Surf. Sci. **110**, 189 – 204 (1981).

[77]H. Xu, J. Aizpurua, M. Käll, and P. Apell, "Electromagnetic contributions to single-molecule sensitivity in surface-enhanced raman scattering," Phys. Rev. E **62**, 4318–4324 (2000).

[78]F. J. García-Vidal and J. B. Pendry, "Collective theory for surface enhanced raman scattering," Phys. Rev. Lett. **77**, 1163–1166 (1996).

[79]E. J. Zeman and G. C. Schatz, "An accurate electromagnetic theory study of surface enhance-

ment factors for Ag, Au, Cu, Li, Na, Ga, In, Zn, and Cd," J. Phys. Chem. **91**, 634–643 (1987).

[80]E. C. Le Ru and P. G. Etchegoin, "Rigorous justifaction of the $|e|^4$ enhancement factor in surface enhanced raman spectroscopy," Chem. Phys. Lett. **423**, 63–66 (2006).

[81]P. Johansson, H. Xu, and M. Käll, "Surface-enhanced raman scattering and fluorescence near metal nanoparticles," Phys. Rev. B **72**, 035427 (2005).

[82]E.-M. Y. e. a. Song Yuan Ding, "Electromagnetic theories of surface-enhanced raman spectroscopy," Chem. Soc. Rev. **46**, 4042–4076 (2017).

[83]V. Amendola, R. Pilot, M. Frasconi, O. M. Maragò, and M. A. Iatì, "Surface plasmon resonance in gold nanoparticles: a review," J. Phys.: Condens. Matter **29**, 203002 (2017).

[84]K. A. Willets and R. P. Van Duyne, "Localized surface plasmon resonance spectroscopy and sensing," Ann. Rev. Phys. Chem. **58**, 267–297 (2007).

[85]M. Moskovits, "Surface-enhanced Raman spectroscopy: a brief retrospective," J. Raman Spectrosc. **36**, 485–496 (2005).

[86]E. C. Le Ru, M. Meyer, E. Blackie, and P. G. Etchegoin, "Advanced aspects of electromagnetic sers enhancement factors at a hot spot," J. Raman Spectrosc. **39**, 1127–1134 (2008).

[87]Y. S. Yamamoto and T. Itoh, "Why and how do the shapes of surface-enhanced raman scattering spectra change? recent progress from mechanistic studies," J. Raman Spectrosc. **47**, 78–88 (2016).

[88]J. Zhao, A. O. Pinchuk, J. M. McMahon, S. Li, L. K. Ausman, A. L. Atkinson, and G. C. Schatz, "Methods for describing the electromagnetic properties of silver and gold nanoparticles," Acc. Chem. Res. **41**, 1710–1720 (2008).

[89]J.-M. Nam, J.-W. Oh, H. Lee, and Y. D. Suh, "Plasmonic nanogap-enhanced raman scattering with nanoparticles," Acc. Chem. Res. **49**, 2746–2755 (2016).

[90]M. Moskovits, "Persistent misconceptions regarding sers," Phys. Chem. Chem. Phys. **15**, 5301–5311 (2013).

[91]D. V. Chulhai, Z. Hu, J. E. Moore, X. Chen, and L. Jensen, "Theory of linear and nonlinear surface-enhanced vibrational spectroscopies," Ann. Rev. Phys. Chem. **67**, 541–564 (2016).

[92]K.-i. Yoshida, T. Itoh, V. Biju, M. Ishikawa, and Y. Ozaki, "Experimental evaluation of the twofold electromagnetic enhancement theory of surface-enhanced resonance raman scattering," Phys. Rev. B **79**, 085419 (2009).

[93]F. W. King, R. P. V. Duyne, and G. C. Schatz, "Theory of raman scattering by molecules adsorbed on electrode surfaces," J. Chem. Phys. **69**, 4472–4481 (1978).

[94]E. Ringe, J. M. McMahon, K. Sohn, C. Cobley, Y. Xia, J. Huang, G. C. Schatz, L. D. Marks, and R. P. Van Duyne, "Unraveling the effects of size, composition, and substrate on the localized surface plasmon resonance frequencies of gold and silver nanocubes: A systematic single-particle approach," J. Phys. Chem. C **114**, 12511–12516 (2010).

[95]J. M. McMahon, S. Li, L. K. Ausman, and G. C. Schatz, "Modeling the effect of small gaps in surface-enhanced raman spectroscopy," J. Phys. Chem. C **116**, 1627–1637 (2012).

[96]M. Barbry, P. Koval, F. Marchesin, R. Esteban, A. G. Borisov, J. Aizpurua, and D. Sánchez-Portal, "Atomistic near-field nanoplasmonics: Reaching atomic-scale resolution in nanooptics," Nano Lett. **15**, 3410–3419 (2015).

[97]S. Trautmann, J. Aizpurua, I. Gotz, A. Undisz, J. Dellith, H. Schneidewind, M. Rettenmayr, and V. Deckert, "A classical description of subnanometer resolution by atomic features in metallic structures," Nanoscale **9**, 391–401 (2017).

[98]D. V. Chulhai and L. Jensen, "Determining molecular orientation with surface-enhanced raman scattering using inhomogenous electric fields," J. Phys. Chem. C **117**, 19622–19631 (2013).

[99]C. C. Neacsu, J. Dreyer, N. Behr, and M. B. Raschke, "Scanning-probe raman spectroscopy with single-molecule sensitivity," Phys. Rev. B **73**, 193406 (2006).

[100]N. Jiang, D. Kurouski, E. A. Pozzi, N. Chiang, M. C. Hersam, and R. P. V. Duyne, "Tip-enhanced raman spectroscopy: From concepts to practical applications," Chem. Phys. Lett. **659**, 16–24 (2016).

[101]I. Alessandri and J. R. Lombardi, "Enhanced raman scattering with dielectrics," Chem. Rev. **116**, 14921–14981 (2016).

[102]K. Frizyuk, M. Hasan, A. Krasnok, A. Alú, and M. Petrov, "Enhancement of raman scattering in dielectric nanostructures with electric and magnetic mie resonances," Phys. Rev. B **97**, 085414 (2018).

[103]J. R. Lombardi and R. L. Birke, "Theory of surface-enhanced raman scattering in semiconductors," J. Phys. Chem. C **118**, 11120–11130 (2014).

[104]G. Schatz, "Electrodynamics of nonspherical noble metal nanoparticles and nanoparticle aggregates," J. Mol. Struct.: THEOCHEM **573**, 73–80 (2001).

[105]S. M. Morton, D. W. Silverstein, and L. Jensen, "Theoretical studies of plasmonics using electronic structure methods," Chem. Rev. **111**, 3962–3994 (2011).

[106]A. Campion and P. Kambhampati, "Surface-enhanced raman scattering," Chem. Soc. Rev. **27**, 241–250 (1998).

[107]L. Jensen, C. M. Aikens, and G. C. Schatz, "Electronic structure methods for studying surface-enhanced raman scattering," Chem. Soc. Rev. **37**, 1061–1073 (2008).

[108]M. Osawa, N. Matsuda, K. Yoshii, and I. Uchida, "Charge transfer resonance raman process in surface-enhanced raman scattering from p-aminothiophenol adsorbed on silver: Herzberg-teller contribution," J. Phys. Chem. **98**, 12702–12707 (1994).

[109]C. Chenal, R. L. Birke, and J. R. Lombardi, "Determination of the degree of charge-transfer contributions to surface-enhanced Raman spectroscopy," ChemPhysChem **9**, 1617–1623 (2008).

[110]J. R. Lombardi, R. L. Birke, L. A. Sanchez, I. Bernard, and S. C. Sun, "The effect of molecular structure on voltage induced shifts of charge transfer excitation in surface enhanced raman scattering," Chem. Phys. Lett. **104**, 240–247 (1984).

[111]J. F. Arenas, J. Soto, I. L. Tocon, D. J. Fernandez, J. C. Otero, and J. I. Marcos, "The role of charge-transfer states of the metal-adsorbate complex in surface-enhanced raman scattering," J. Chem. Phys. **116**, 7207–7216 (2002).

[112]B. Giese and D. McNaughton, "Surface-enhanced raman spectroscopic study of uracil. the influence of the surface substrate, surface potential, and ph," J. Phys. Chem. B **106**, 1461–1470 (2002).

[113]E. Bailo and V. Deckert, "Tip-enhanced Raman scattering," Chem. Soc. Rev. **37**, 921–930 (2008).

[114]R. M. Stöckle, Y. D. Suh, V. Deckert, and R. Zenobi, "Nanoscale chemical analysis by tip-enhanced raman spectroscopy," Chem. Phys. Lett. **318**, 131–136 (2000).

[115]B. Pettinger, K. F. Domke, D. Zhang, G. Picardi, and R. Schuster, "Tip-enhanced raman scattering: Influence of the tip-surface geometry on optical resonance and enhancement," Surf. Sci. **603**, 1335–1341 (2009).

[116]M. Sun, Y. Fang, Z. Yang, and H. Xu, "Chemical and electromagnetic mechanisms of tip-enhanced raman scattering," Phys. Chem. Chem. Phys. **11**, 9412–9419 (2009).

[117]A. L. Demming, F. Festy, and D. Richards, "Plasmon resonances on metal tips: Understanding tip-enhanced raman scattering," J. Chem. Phys. **122**, 184716 (2005).

[118]E. A. Pozzi, G. Goubert, N. Chiang, N. Jiang, C. T. Chapman, M. O. McAnally, A.-I. Henry, T. Seideman, G. C. Schatz, M. C. Hersam, and R. P. V. Duyne, "Ultrahigh-vacuum tip-enhanced raman spectroscopy," Chem. Rev. **117**, 4961–4982 (2017).

[119]P. Verma, "Tip-enhanced raman spectroscopy: Technique and recent advances," Chem. Rev.

117, 6447–6466 (2017).

[120]R. R. Jones, D. C. Hooper, L. Zhang, D. Wolverson, and V. K. Valev, "Raman techniques: Fundamentals and frontiers," Nanoscale Res. Lett. **14**, 231 (2019).

[121]M. D. Sonntag, J. M. Klingsporn, L. K. Garibay, J. M. Roberts, J. A. Dieringer, T. Seideman, K. A. Scheidt, L. Jensen, G. C. Schatz, and R. P. Van Duyne, "Single-molecule tip-enhanced raman spectroscopy," J. Phys. Chem. C **116**, 478–483 (2012).

[122]B. Pettinger, B. Ren, G. Picardi, R. Schuster, and G. Ertl, "Nanoscale probing of adsorbed species by tip-enhanced raman spectroscopy," Phys. Rev. Lett. **92**, 096101 (2004).

[123]Z. Zhang, S. Sheng, R. Wang, and M. Sun, "Tip-enhanced raman spectroscopy," Anal. Chem. **88**, 9328–9346 (2016).

[124]N. J. Halas, S. Lal, W.-S. Chang, S. Link, and P. Nordlander, "Plasmons in strongly coupled metallic nanostructures," Chem. Rev. **111**, 3913–3961 (2011).

[125]L. L. Zhao, L. Jensen, and G. C. Schatz, "Surface-enhanced raman scattering of pyrazine at the junction between two ag20 nanoclusters," Nano Lett. **6**, 1229–1234 (2006).

[126]D. Marinica, A. Kazansky, P. Nordlander, J. Aizpurua, and A. G. Borisov, "Quantum plasmonics: Nonlinear effects in the field enhancement of a plasmonic nanoparticle dimer," Nano Lett. **12**, 1333–1339 (2012).

[127]C. Readman, B. de Nijs, I. Szabó, A. Demetriadou, R. Greenhalgh, C. Durkan, E. Rosta, O. A. Scherman, and J. J. Baumberg, "Anomalously large spectral shifts near the quantum tunnelling limit in plasmonic rulers with subatomic resolution," Nano Lett. **19**, 2051–2058 (2019).

[128]R. Esteban, A. G. Borisov, P. Nordlander, and J. Aizpurua, "Bridging quantum and classical plasmonics with a quantum-corrected model," Nat Commun. **3**, 825 (2012).

[129]K. J. Savage, M. M. Hawkeye, R. Esteban, A. G. Borisov, J. Aizpurua, and J. J. Baumberg, "Revealing the quantum regime in tunnelling plasmonics," Nature **491**, 574–577 (2012).

[130]J. H. Yoon, Y. Zhou, M. G. Blaber, G. C. Schatz, and S. Yoon, "Surface plasmon coupling of compositionally heterogeneous core-satellite nanoassemblies," J. Phys. Chem. Lett. **4**, 1371–1378 (2013).

[131]J. Zuloaga, E. Prodan, and P. Nordlander, "Quantum plasmonics: Optical properties and tunability of metallic nanorods," ACS Nano **4**, 5269–5276 (2010).

[132]P. Liu, D. V. Chulhai, and L. Jensen, "Atomistic characterization of plasmonic dimers in the quantum size regime," J. Phys. Chem. C **123**, 13900–13907 (2019).

[133]D.-J. Yang, S. Zhang, S.-J. Im, Q.-Q. Wang, H. Xu, and S. Gao, "Analytical analysis of spectral

sensitivity of plasmon resonances in a nanocavity," Nanoscale **11**, 10977–10983 (2019).

[134]S. F. Tan, L. Wu, J. K. W. Yang, P. Bai, M. Bosman, and C. A. Nijhuis, "Quantum Plasmon Resonances Controlled by Molecular Tunnel Junctions," Science **343**, 1496–1499 (2014).

[135]R. T. Hill, J. J. Mock, A. Hucknall, S. D. Wolter, N. M. Jokerst, D. R. Smith, and A. Chilkoti, "Plasmon ruler with angstrom length resolution," ACS Nano **6**, 9237–9246 (2012).

[136]D.-Y. Wu, J.-F. Li, B. Ren, and Z.-Q. Tian, "Electrochemical surface-enhanced raman spectroscopy of nanostructures," Chem. Soc. Rev. **37**, 1025–1041 (2008).

[137]S. Sun and P. Wu, "Competitive surface-enhanced raman scattering effects in noble metal nanoparticle-decorated graphene sheets," Phys. Chem. Chem. Phys. **13**, 21116–21120 (2011).

[138]R. Esteban, A. Zugarramurdi, P. Zhang, P. Nordlander, F. J. Garcia-Vidal, A. G. Borisov, and J. Aizpurua, "A classical treatment of optical tunneling in plasmonic gaps: extending the quantum corrected model to practical situations," Faraday Discuss. **178**, 151–183 (2015).

[139]C. Chen, N. Hayazawa, and S. Kawata, "A 1.7 nm resolution chemical analysis of carbon nanotubes by tip-enhanced raman imaging in the ambient," Nat Commun. **5**, 3312 (2014).

[140]E. M. van Schrojenstein Lantman, T. Deckert-Gaudig, A. J. G. Mank, V. Deckert, and B. M. Weckhuysen, "Catalytic processes monitored at the nanoscale with tip-enhanced raman spectroscopy," Nat. Nanotechnol. **7**, 583–586 (2012).

[141]R. Zhang, Y. Zhang, Z. C. Dong, S. Jiang, C. Zhang, L. G. Chen, L. Zhang, Y. Liao, J. Aizpurua, Y. Luo, J. L. Yang, and J. G. Hou, "Chemical mapping of a single molecule by plasmon-enhanced raman scattering," Nature **498**, 82–86 (2013).

[142]X. Wang, S.-C. Huang, T.-X. Huang, H.-S. Su, J.-H. Zhong, Z.-C. Zeng, M.-H. Li, and B. Ren, "Tip-enhanced raman spectroscopy for surfaces and interfaces," Chem. Soc. Rev. **46**, 4020–4041 (2017).

[143]J. Lee, K. T. Crampton, N. Tallarida, and V. A. Apkarian, "Visualizing vibrational normal modes of a single molecule with atomically confined light," Nature **568**, 78–82 (2019).

[144]N. Tallarida, J. Lee, and V. A. Apkarian, "Tip-Enhanced Raman Spectromicroscopy on the Angstrom Scale: Bare and CO-Terminated Ag Tips," ACS Nano **11**, 11393–11401 (2017).

[145]J. Lee, N. Tallarida, X. Chen, P. Liu, L. Jensen, and V. A. Apkarian, "Tip-enhanced raman spectromicroscopy of co(ii)-tetraphenylporphyrin on au(111): Toward the chemists' microscope," ACS Nano **11**, 11466–11474 (2017).

[146]N. Chiang, X. Chen, G. Goubert, D. V. Chulhai, X. Chen, E. A. Pozzi, N. Jiang, M. C. Hersam, T. Seideman, L. Jensen, and R. P. Van Duyne, "Conformational contrast of surface-mediated

molecular switches yields ångstrom-scale spatial resolution in ultrahigh vacuum tip-enhanced raman spectroscopy," Nano Lett. **16**, 7774–7778 (2016).

[147]T. Schmid, B.-S. Yeo, G. Leong, J. Stadler, and R. Zenobi, "Performing tip-enhanced raman spectroscopy in liquids," J. Raman Spectrosc. **40**, 1392–1399 (2009).

[148]N. Martín Sabanés, L. M. A. Driessen, and K. F. Domke, "Versatile side-illumination geometry for tip-enhanced raman spectroscopy at solid/liquid interfaces," Anal. Chem. **88**, 7108–7114 (2016).

[149]Z.-C. Zeng, S.-C. Huang, D.-Y. Wu, L.-Y. Meng, M.-H. Li, T.-X. Huang, J.-H. Zhong, X. Wang, Z.-L. Yang, and B. Ren, "Electrochemical tip-enhanced raman spectroscopy," J. Am. Chem. Soc. **137**, 11928–11931 (2015).

[150]D. Kurouski, M. Mattei, and R. P. V. Duyne, "Probing redox reactions at the nanoscale with electrochemical tip-enhanced raman spectroscopy," Nano Lett. **15**, 7956–7962 (2015).

[151]M. Mattei, G. Kang, G. Goubert, D. V. Chulhai, G. C. Schatz, L. Jensen, and R. P. V. Duyne, "Tip-enhanced raman voltammetry: Coverage dependence and quantitative modeling," Nano Lett. **17**, 590–596 (2017).

[152]S. Zaleski, A. J. Wilson, M. Mattei, X. Chen, G. Goubert, M. F. Cardinal, K. A. Willets, and R. P. Van Duyne, "Investigating nanoscale electrochemistry with surface- and tip-enhanced raman spectroscopy," Acc. Chem. Res. **49**, 2023–2030 (2016).

[153]G. Picardi, A. Królikowska, R. Yasukuni, M. Chaigneau, M. Escude, V. Mourier, C. Licitra, and R. Ossikovski, "Exchange of methyl- and azobenzene-terminated alkanethiols on polycrystalline gold studied by tip-enhanced raman mapping," ChemPhysChem **15**, 276–282 (2014).

[154]X. Wang, W. Shi, G. She, and L. Mu, "Surface-enhanced raman scattering (sers) on transition metal and semiconductor nanostructures," Phys. Chem. Chem. Phys. **14**, 5891–5901 (2012).

[155]G. Demirel, R. L. M. Gieseking, R. Ozdemir, S. Kahmann, M. A. Loi, G. C. Schatz, A. Facchetti, and H. Usta, "Molecular engineering of organic semiconductors enables noble metal-comparable sers enhancement and sensitivity," Nat Commun. **10**, 5502 (2019).

[156]J. R. Lombardi, "The theory of surface-enhanced raman scattering on semiconductor nanoparticles; toward the optimization of sers sensors," Faraday Discuss. **205**, 105–120 (2017).

[157]A. K. Kuhlman and A. T. Zayak, "Revealing interaction of organic adsorbates with semiconductor surfaces using chemically enhanced raman," J. Phys. Chem. Lett. **5**, 964–968 (2014).

[158]X. X. Han, W. Ji, B. Zhao, and Y. Ozaki, "Semiconductor-enhanced raman scattering: active nanomaterials and applications," Nanoscale **9**, 4847–4861 (2017).

[159]L. G. Quagliano, "Observation of molecules adsorbed on iii-v semiconductor quantum dots by surface-enhanced raman scattering," J. Am. Chem. Soc. **126**, 7393–7398 (2004).

[160]M. Yilmaz, E. Babur, M. Ozdemir, R. L. Gieseking, Y. Dede, U. Tamer, G. C. Schatz, A. Facchetti, H. Usta, and G. Demirel, "Nanostructured organic semiconductor films for molecular detection with surface-enhanced raman spectroscopy," Nat. Mater. **16**, 918 (2017).

[161]X. Ling, W. Fang, Y.-H. Lee, P. T. Araujo, X. Zhang, J. F. Rodriguez-Nieva, Y. Lin, J. Zhang, J. Kong, and M. S. Dresselhaus, "Raman enhancement effect on two-dimensional layered materials: Graphene, h-bn and mos2," Nano Lett. **14**, 3033–3040 (2014).

[162]X. Ling, L. Xie, Y. Fang, H. Xu, H. Zhang, J. Kong, M. S. Dresselhaus, J. Zhang, and Z. Liu, "Can graphene be used as a substrate for raman enhancement?" Nano Lett. **10**, 553–561 (2010).

[163]W. Xu, X. Ling, J. Xiao, M. S. Dresselhaus, J. Kong, H. Xu, Z. Liu, and J. Zhang, "Surface enhanced raman spectroscopy on a flat graphene surface," Proc. Natl. Acad. Sci. USA **109**, 9281–9286 (2012).

[164]W. Xu, N. Mao, and J. Zhang, "Graphene: A platform for surface-enhanced raman spectroscopy," Small **9**, 1206–1224 (2013).

[165]S. Huang, X. Ling, L. Liang, Y. Song, W. Fang, J. Zhang, J. Kong, V. Meunier, and M. S. Dresselhaus, "Molecular selectivity of graphene-enhanced raman scattering," Nano Lett. **15**, 2892–2901 (2015).

[166]F. Schedin, E. Lidorikis, A. Lombardo, V. G. Kravets, A. K. Geim, A. N. Grigorenko, K. S. Novoselov, and A. C. Ferrari, "Surface-enhanced raman spectroscopy of graphene," ACS Nano **4**, 5617–5626 (2010).

[167]Y. Wang, W. Ruan, J. Zhang, B. Yang, W. Xu, B. Zhao, and J. R. Lombardi, "Direct observation of surface-enhanced raman scattering in zno nanocrystals," J. Raman Spectrosc. **40**, 1072–1077 (2009).

[168]A. Musumeci, D. Gosztola, T. Schiller, N. M. Dimitrijevic, V. Mujica, D. Martin, and T. Rajh, "Sers of semiconducting nanoparticles (tio2 hybrid composites)," J. Am. Chem. Soc. **131**, 6040–6041 (2009).

[169]I. Alessandri, "Enhancing raman scattering without plasmons: Unprecedented sensitivity achieved by tio2 shell-based resonators," J. Am. Chem. Soc. **135**, 5541–5544 (2013).

[170]N. Bontempi, I. Vassalini, and I. Alessandri, "All-dielectric core/shell resonators: From plasmon-free sers to multimodal analysis," J. Raman Spectrosc. **49**, 943–953 (2018).

[171]X. Song, Y. Wang, F. Zhao, Q. Li, H. Q. Ta, M. H. Rümmeli, C. G. Tully, Z. Li, W.-J. Yin,

L. Yang, K.-B. Lee, J. Yang, I. Bozkurt, S. Liu, W. Zhang, and M. Chhowalla, "Plasmon-free surface-enhanced raman spectroscopy using metallic 2d materials," ACS Nano **13**, 8312–8319 (2019).

[172]L. Tao, K. Chen, Z. Chen, C. Cong, C. Qiu, J. Chen, X. Wang, H. Chen, T. Yu, W. Xie, S. Deng, and J.-B. Xu, "1t' transition metal telluride atomic layers for plasmon-free sers at femtomolar levels," J. Am. Chem. Soc. **140**, 8696–8704 (2018).

[173]L. Sun, H. Hu, D. Zhan, J. Yan, L. Liu, J. S. Teguh, E. K. L. Yeow, P. S. Lee, and Z. Shen, "Plasma modified mos2 nanoflakes for surface enhanced raman scattering," Small **10**, 1090–1095 (2014).

[174]P. Miao, J.-K. Qin, Y. Shen, H. Su, J. Dai, B. Song, Y. Du, M. Sun, W. Zhang, H.-L. Wang, C.-Y. Xu, and P. Xu, "Unraveling the raman enhancement mechanism on 1t'-phase res2 nanosheets," Small **14**, 1704079 (2018).

[175]Y. Lee, H. Kim, J. Lee, S. H. Yu, E. Hwang, C. Lee, J.-H. Ahn, and J. H. Cho, "Enhanced raman scattering of rhodamine 6g films on two-dimensional transition metal dichalcogenides correlated to photoinduced charge transfer," Chem. Mater. **28**, 180–187 (2016).

[176]C. Muehlethaler, C. R. Considine, V. Menon, W.-C. Lin, Y.-H. Lee, and J. R. Lombardi, "Ultrahigh raman enhancement on monolayer mos2," ACS Photonics **3**, 1164–1169 (2016).

[177]G. Zheng, P. Zhang, S. Zhang, Y. Peng, L. Huang, L. Zhang, Y. Jin, Z. Jiao, and X. Sun, "Sers effect of selectively adsorbed dyes by hydrothermally-produced mos2 nanosheets," New J. Chem. **42**, 18906–18912 (2018).

[178]D. Maznichenko, K. Venkatakrishnan, and B. Tan, "Stimulating multiple sers mechanisms by a nanofibrous three-dimensional network structure of titanium dioxide (tio2)," J. Phys. Chem. C **117**, 578–583 (2013).

[179]W. Li, R. Zamani, P. Rivera Gil, B. Pelaz, M. Ibáñez, D. Cadavid, A. Shavel, R. A. Alvarez-Puebla, W. J. Parak, J. Arbiol, and A. Cabot, "Cute nanocrystals: Shape and size control, plasmonic properties, and use as sers probes and photothermal agents," J. Am. Chem. Soc. **135**, 7098–7101 (2013).

[180]S. K. Islam, M. Tamargo, R. Moug, and J. R. Lombardi, "Surface-enhanced raman scattering on a chemically etched znse surface," J. Phys. Chem. C **117**, 23372–23377 (2013).

[181]M. Liu and W. Chen, "Graphene nanosheets-supported ag nanoparticles for ultrasensitive detection of tnt by surface-enhanced raman spectroscopy," Biosens. Bioelectron. **46**, 68–73 (2013).

[182]E. B. Barros and M. S. Dresselhaus, "Theory of raman enhancement by two-dimensional ma-

terials: Applications for graphene-enhanced raman spectroscopy," Phys. Rev. B **90**, 035443 (2014).

[183]S. J. Hurst, H. C. Fry, D. J. Gosztola, and T. Rajh, "Utilizing chemical raman enhancement: A route for metal oxide support-based biodetection," J. Phys. Chem. C **115**, 620–630 (2011).

[184]W. Ji, Y. Kitahama, X. Han, X. Xue, Y. Ozaki, and B. Zhao, "ph-dependent sers by semiconductor-controlled charge-transfer contribution," J. Phys. Chem. C **116**, 24829–24836 (2012).

[185]R. M. Hexter and M. G. Albrecht, "Metal surface raman spectroscopy: Theory," Spectrochim. Acta A **35**, 233–251 (1979).

[186]E. Burstein, Y. J. Chen, C. Y. Chen, S. Lundquist, and E. Tosatti, ""giant" raman scattering by adsorbed molecules on metal surfaces," Solid State Commun. **29**, 567–570 (1979).

[187]M. J. Weaver, S. Farquharson, and M. A. Tadayyoni, "Surface enhancement factors for raman scattering at silver electrodes. role of adsorbate–surface interactions and electronic structure," J. Chem. Phys. **82**, 4867–4874 (1985).

[188]P. Avouris and J. E. Demuth, "Electronic excitations of benzene, pyridine, and pyrazine adsorbed on ag(111)," J. Chem. Phys. **75**, 4783–4794 (1981).

[189]R. A. Wolkow and M. Moskovits, "A comparative study of the electron energy loss spectrum and the surface-enhance raman spectrum of benzene adsorbed on silver," J. Chem. Phys. **96**, 3966–3980 (1992).

[190]P. Kambhampati, C. M. Child, M. C. Foster, and A. Campion, "On the chemical mechanism of surface enhanced raman scattering: Experiment and theory," J. Chem. Phys. **108**, 5013–5026 (1998).

[191]F. J. Adrian, "Charge transfer effects in surface-enhanced raman scattering," J. Chem. Phys. **77**, 5302–5314 (1982).

[192]J. F. Arenas, M. S. Woolley, I. L. Tocón, J. C. Otero, and J. I. Marcos, "Complete analysis of the surface-enhanced raman scattering of pyrazine on the silver electrode on the basis of a resonant charge transfer mechanism involving three states," J. Chem. Phys. **112**, 7669–7683 (2000).

[193]J. F. Arenas, M. S. Woolley, J. C. Otero, and J. I. Marcos, "Charge-transfer processes in surface-enhanced Raman scattering. Franck-Condon active vibrations of pyrazine," J. Phys. Chem. **100**, 3199–3206 (1996).

[194]J. F. Arenas, I. Lopez Tocon, J. C. Otero, and J. I. Marcos, "Charge-transfer processes in

surface-enhanced Raman scattering. Franck-Condon active vibrations of pyridine," J. Phys. Chem. **100**, 9254–9261 (1996).

[195]F. Avila, J. Soto, J. F. Arenas, J. A. Rodríguez, D. Peláez, and J. C. Otero, "Outstanding role of silver nanoparticles in the surface-enhanced resonance raman scattering of p-benzosemiquinone," J. Phys. Chem. C **113**, 105–108 (2009).

[196]M. R. Lopez-Ramirez, C. Ruano, J. L. Castro, J. F. Arenas, J. Soto, and J. C. Otero, "Surface-enhanced raman scattering of benzoate anion adsorbed on silver nanoclusters: Evidence of the transient formation of the radical dianion," J. Phys. Chem. C **114**, 7666–7672 (2010).

[197]J. F. Arenas, D. J. Fernández, J. Soto, I. López-Tocón, and J. C. Otero, "Role of the electrode potential in the charge-transfer mechanism of surface-enhanced raman scattering," J. Phys. Chem. B **107**, 13143–13149 (2003).

[198]S. P. Centeno, I. Lópex-Tocón, J. F. Arenas, J. Soto, and J. C. Otero, "Selection rules of the charge transfer mechanism of surface-enhanced Raman scattering: The effect of the adsorption on the relative intensities of pyrimidine bonded to silver nanoclusters," J. Phys. Chem. B **110**, 14916–14922 (2006).

[199]J. Arenas, J. Soto, D. Pelaez, D. Fernandez, and J. Otero, "Understanding complex surface-enhanced raman scattering, using quantum chemical calculations," Int. J. Quantum Chem. **104**, 681–694 (2005).

[200]R. L. Birke, J. R. Lombardi, and J. I. Gersten, "Observation of a continuum in enhanced raman scattering from a metal-solution interface," Phys. Rev. Lett. **43**, 71–75 (1979).

[201]J. I. Gersten, R. L. Birke, and J. R. Lombardi, "Theory of enhancedi light scattering from molecules adsorbed at the metal-solution interface," Phys. Rev. Lett. **43**, 147–150 (1979).

[202]Y.-X. Chen and A. Otto, "Electronic effects in sers by liquid water," J. Raman Spectrosc. **36**, 736–747 (2005).

[203]D. M. NEWNS, "Self-consistent model of hydrogen chemisorption," Phys. Rev. **178**, 1123–1135 (1969).

[204]B. Persson, "On the theory of surface-enhanced raman scattering," Chem. Phys. Lett. **82**, 561–565 (1981).

[205]A. Otto, "Raman spectra of (cn)- adsorbed at a silver surface," Surf. Sci. **75**, L392–L396 (1978).

[206]J. Billmann, G. Kovacs, and A. Otto, "Enhanced raman effect from cyanide adsorbed on a silver electrode," Surf. Sci. **92**, 153–173 (1980).

[207]J. Billman and A. Otto, "Charge transfer between adsorbed cyanide and silver probed by sers,"

Surf. Sci. **138**, 1–25 (1984).

[208]A. Otto, J. Billmann, J. Eickmans, U. Ertürk, and C. Pettenkofer, "The "adatom model" of sers (surface enhanced raman scattering): The present status," Surf. Sci. **138**, 319–338 (1984).

[209]C. Pettenkofer, J. Eickmans, U. Ertürk, and A. Otto, "On the nature of "sers active sites"," Surf. Sci. **151**, 9–36 (1985).

[210]C. Pettenkofer and A. Otto, ""chemical effects" of vibrational lifetime and frequency of co on ag," Surf. Sci. **151**, 37–51 (1985).

[211]J. Billmann and A. Otto, "Electronic surface state contribution to surface enhanced raman scattering," Solid State Commun. **44**, 105–107 (1982).

[212]A. Otto, J. Timper, J. Billmann, and I. Pockrand, "Enhanced inelastic light scattering from metal electrodes caused by adatoms," Phys. Rev. Lett. **45**, 46–49 (1980).

[213]A. Otto, I. Mrozek, H. Grabhorn, and W. Akemann, "Surface-enhanced Raman scattering," J. Phys.: Condens. Matter **4**, 1143–1212 (1992).

[214]A. Otto, "Surface-enhanced raman scattering of adsorbates," J. Raman Spectrosc. **22**, 743–752 (1991).

[215]A. Otto, "The 'chemical' (electronic) contribution to surface-enhanced raman scattering," J. Raman Spectrosc. **36**, 497–509 (2005).

[216]A. Otto, M. Lust, A. Pucci, and G. Meyer, ""sers active sites", facts, and open questions," Can. J. Anal. Sci. Spectrosc. **52**, 150–171 (2007).

[217]L. Cui, D.-Y. Wu, A. Wang, B. Ren, and Z.-Q. Tian, "Charge-transfer enhancement involved in the sers of adenine on rh and pd demonstrated by ultraviolet to visible laser excitation," J. Phys. Chem. C **114**, 16588–16595 (2010).

[218]J. T. Hupp, D. Larkin, and M. J. Weaver, "Specific adsorption of halide and pseudohalide ions at electrochemically roughened versus smooth silver-aqueous interfaces," Surf. Sci. **125**, 429–451 (1983).

[219]P. K. K. Pandey and G. C. Schatz, "Time-dependent hartree–fock calculations of surface-enhanced raman intensities. h2 adsorbed on a model li cluster," Chem. Phys. Lett. **88**, 193–197 (1982).

[220]P. K. K. Pandey and G. C. Schatz, "A detailed analysis of the raman enhancement mechanisms associated with the interaction of a raman scatterer with a resonant metal cluster: Results for lin-h2," J. Chem. Phys. **80**, 2959–2972 (1984).

[221]L. Zhao, L. Jensen, and G. C. Schatz, "Pyridine-Ag_{20} cluster: A model system for studying

surface-enhanced raman scattering," J. Am. Chem. Soc. **128**, 2911–2919 (2006).

[222]S. M. Morton and L. Jensen, "Understanding the molecule-surface chemical coupling in SERS," J. Am. Chem. Soc. **131**, 4090–4098 (2009).

[223]J. E. Moore, S. M. Morton, and L. Jensen, "Importance of correctly describing charge-transfer excitations for understanding the chemical effect in sers," J. Phys. Chem. Lett. **3**, 2470–2475 (2012).

[224]N. Valley, N. Greeneltch, R. P. Van Duyne, and G. C. Schatz, "A look at the origin and magnitude of the chemical contribution to the enhancement mechanism of surface-enhanced raman spectroscopy (SERS): Theory and experiment," J. Phys. Chem. Lett. **4**, 2599–2604 (2013).

[225]R. L. M. Gieseking, J. Lee, N. Tallarida, V. A. Apkarian, and G. C. Schatz, "Bias-dependent chemical enhancement and nonclassical stark effect in tip-enhanced raman spectromicroscopy of co-terminated ag tips," J. Phys. Chem. Lett. **9**, 3074–3080 (2018).

[226]R. L. Gieseking, M. A. Ratner, and G. C. Schatz, "Semiempirical modeling of electrochemical charge transfer," Faraday Discuss. **199**, 547–563 (2017).

[227]R. L. Gieseking, M. A. Ratner, and G. C. Schatz, "Theoretical modeling of voltage effects and the chemical mechanism in surface-enhanced raman scattering," Faraday Discuss. **205**, 149–171 (2017).

[228]L. Chen, Y. Gao, Y. Cheng, H. Li, Z. Wang, Z. Li, and R.-Q. Zhang, "Nonresonant chemical mechanism in surface-enhanced raman scattering of pyridine on m@au12 clusters," Nanoscale **8**, 4086–4093 (2016).

[229]X. Zhao and M. Chen, "Dft study on the influence of electric field on surface-enhanced raman scattering from pyridine-metal complex," J. Raman Spectrosc. **45**, 62–67 (2014).

[230]C. M. Aikens and G. C. Schatz, "TDDFT studies of absorption and SERS spectra of pyridine interacting with Au_20," J. Phys. Chem. A **110**, 13317–13324 (2006).

[231]L. Jensen, L. L. Zhao, and G. C. Schatz, "Size-dependence of the enhanced Raman scattering of pyridine adsorbed on Ag_n (n = 2-8, 20) clusters," J. Phys. Chem. C **111**, 4756–4764 (2007).

[232]D.-Y. Wu, S. Duan, B. Ren, and Z.-Q. Tian, "Density functional theory study of surface-enhanced Raman scattering spectra of pyridine adsorbed on noble and transition metal surfaces," J. Raman Spectrosc. **36**, 533–540 (2005).

[233]M. Sun, S. Wan, Y. Liu, Y. Jia, and H. Xu, "Chemical mechanism of surface-enhanced resonance raman scattering via charge transfer in pyridine-Ag_2 complex," J. Raman Spectrosc. **39**, 402–408 (2008).

[234]D. Wu, B. Ren, Y. Jiang, X. Xu, and Z. Tian, "Density functional study and normal-mode analysis of the bindings and vibrational frequency shifts of the pyridine-M (M = Cu, Ag, Au, Cu+, Ag+, Au+, and Pt) complexes," J. Phys. Chem. A **106**, 9042–9052 (2002).

[235]D.-Y. Wu, X.-M. Liu, S. Duan, X. Xu, B. Ren, S.-H. Lin, and Z.-Q. Tian, "Chemical enhancement effects in SERS spectra: A quantum chemical study of pyridine interacting with copper, silver, gold and platinum metals," J. Phys. Chem. C **112**, 4195–4204 (2008).

[236]G. Cardini and M. Muniz-Miranda, "Density functional study on the adsorption of pyrazole onto silver colloidal particles," J. Phys. Chem. B **106**, 6875–6880 (2002).

[237]M. Muniz-Miranda, G. Cardini, M. Pagliai, and V. Schettino, "DFT investigation on the SERS band at $\sim$1025 cm^{-1} of pyridine adsorbed on silver," Chem. Phys. Lett. **436**, 179–183 (2007).

[238]G. Cardini, M. Muniz-Miranda, M. Pagliai, and V. Schettino, "A density functional study of the SERS spectra of pyridine adsorbed on silver clusters," Theor. Chim. Acta **117**, 451–458 (2007).

[239]P. Johansson, "Illustrative direct *ab initio* calculations of surface Raman spectra," Phys. Chem. Chem. Phys. **7**, 475–482 (2005).

[240]S. K. Saikin, R. Olivares-Amaya, D. Rappoport, M. Stopa, and A. Aspuru-Guzik, "On the chemical bonding effects in the raman response: Benzenethiol adsorbed on silver clusters," Phys. Chem. Chem. Phys. **11**, 9401–9411 (2009).

[241]M. J. Trujillo, J. C. Becca, S. L. Strausser, and et al., "Using SERS to understand the binding of n-heterocyclic carbenes to gold surfaces," J. Phys. Chem. Lett. **9**, 6779–6785 (2018).

[242]A. Królikowska, J. Cukras, M. Witkowski, D. Tymecka, A. Hernik-Magoń, A. Misicka, and W. Dzwolak, "Sers and dft study of noble-metal-anchored cys-trp/trp-cys dipeptides: Influence of main-chain direction and terminal modifications," J. Phys. Chem. C **124**, 7097–7116 (2020).

[243]A. T. Zayak, Y. S. Hu, H. Choo, J. Bokor, S. Cabrini, P. J. Schuck, and J. B. Neaton, "Chemical raman enhancement of organic adsorbates on metal surfaces," Phys. Rev. Lett. **106**, 083003 (2011).

[244]A. T. Zayak, H. Choo, Y. S. Hu, D. J. Gargas, S. Cabrini, J. Bokor, P. J. Schuck, and J. B. Neaton, "Harnessing chemical raman enhancement for understanding organic adsorbate binding on metal surfaces," J. Phys. Chem. Lett. **3**, 1357–1362 (2012).

[245]F. W. Hilty, A. K. Kuhlman, F. Pauly, and A. T. Zayak, "Raman scattering from a molecule-semiconductor interface tuned by an electric field: Density functional theory approach," J. Phys. Chem. C **119**, 23113–23118 (2015).

[246]W. Hu, S. Duan, G. Zhang, Y. Ma, G. Tian, and Y. Luo, "Quasi-analytical approach for modeling of surface-enhanced raman scattering," J. Phys. Chem. C **119**, 28992–28998 (2015).

[247]J. R. Lombardi, R. L. Birke, T. Lu, and J. Xu, "Charge-transfer theory of surface enhanced raman spectroscopy: Herzberg–teller contributions," J. Chem. Phys. **84**, 4174–4180 (1986).

[248]J. R. Lombardi and R. L. Birke, "Time-dependent picture of the charge-transfer contributions to surface enhanced raman spectroscopy," J. Chem. Phys. **126**, 244709 (2007).

[249]J. R. Lombardi and R. L. Birke, "The theory of surface-enhanced raman scattering," J. Chem. Phys. **136**, 144704 (2012).

[250]R. L. Birke and J. R. Lombardi, "Relative contributions of franck–condon to herzberg–teller terms in charge transfer surface-enhanced raman scattering spectroscopy," J. Chem. Phys. **152**, 224107 (2020).

[251]J. R. Lombardi and R. L. Birke, "A unified view of surface-enhanced raman scattering," Acc. Chem. Res. **42**, 734–742 (2009).

[252]J. R. Lombardi and R. L. Birke, "A unified approach to surface-enhanced Raman spectroscopy," J. Phys. Chem. C **112**, 5605–5617 (2008).

[253]L. Liu, D. Chen, H. Ma, and W. Liang, "Spectral characteristics of chemical enhancement on sers of benzene-like derivatives: Franck–condon and herzberg–teller contributions," J. Phys. Chem. C **119**, 27609–27619 (2015).

[254]H. Ma, J. Liu, and W. Liang, "Time-dependent approach to resonance raman spectra including duschinsky rotation and herzberg–teller effects: Formalism and its realistic applications," J. Chem. Theor. Comput. **8**, 4474–4482 (2012).

[255]J. Guthmuller, "Comparison of simplified sum-over-state expressions to calculate resonance raman intensities including franck-condon and herzberg-teller effects," J. Chem. Phys. **144**, 064106 (2016).

[256]G. R. Erdheim, R. L. Birke, and J. R. Lombardi, "Surface enhanced raman spectrum of pyrazine. observation of forbidden lines at the electrode surface," Chem. Phys. Lett. **69**, 495–498 (1980).

[257]R. L. Birke, V. Znamenskiy, and J. R. Lombardi, "A charge-transfer surface enhanced raman scattering model from time-dependent density functional theory calculations on a ag_{10}-pyridine complex," J. Chem. Phys. **132**, 214707 (2010).

[258]R. L. Birke, J. R. Lombardi, W. A. Saidi, and P. Norman, "Surface-enhanced raman scattering due to charge-transfer resonances: A time-dependent density functional theory study of ag13-

4-mercaptopyridine," J. Phys. Chem. C **120**, 20721–20735 (2016).

[259]A. Vivoni, R. Birke, R. Foucault, and J. Lombardi, "*Ab Initio* frequency calculations of pyridine adsorbed on an adatom model of a SERS active site of a silver surface," J. Phys. Chem. B **107**, 5547–5557 (2003).

[260]M. V. Cañamares, C. Chenal, R. L. Birke, and J. R. Lombardi, "Dft, sers, and single-molecule sers of crystal violet," J. Phys. Chem. C **112**, 20295–20300 (2008).

[261]B. Pettinger, "Light scattering by adsorbates at ag particles: Quantum-mechanical approach for energy transfer induced interfacial optical processes involving surface plasmons, multipoles, and electron-hole pairs," J. Chem. Phys. **85**, 7442–7451 (1986).

[262]A. Jorio, N. S. Mueller, and S. Reich, "Symmetry-derived selection rules for plasmon-enhanced raman scattering," Phys. Rev. B **95**, 155409 (2017).

[263]J. Roman-Perez, C. Ruano, S. P. Centeno, I. López-Tocón, J. F. Arenas, J. Soto, and J. C. Otero, "Huge energy gain in metal-to-molecule charge transfer processes: A combined effect of an electrical capacitive enhancement in nanometer-size hot spots and the electronic structure of the surface complex," J. Phys. Chem. C **118**, 2718–2725 (2014).

[264]V. N. Pustovit and T. V. Shahbazyan, "Microscopic theory of surface-enhanced raman scattering in noble-metal nanoparticles," Phys. Rev. B **73**, 085408 (2006).

[265]N. S. Mueller, S. Heeg, and S. Reich, "Surface-enhanced raman scattering as a higher-order raman process," Phys. Rev. A **94**, 023813 (2016).

[266]H. Xu, X.-H. Wang, M. P. Persson, H. Q. Xu, M. Käll, and P. Johansson, "Unified treatment of fluorescence and raman scattering processes near metal surfaces," Phys. Rev. Lett. **93**, 243002 (2004).

[267]M. Mohammadpour, M. H. Khodabandeh, L. Visscher, and Z. Jamshidi, "Elucidation of charge-transfer sers selection rules by considering the excited state properties and the role of electrode potential," Phys. Chem. Chem. Phys. **19**, 7833–7843 (2017).

[268]D. Aranda, J. Román-Pérez, I. López-Tocón, J. Soto, F. Avila, and J. C. Otero, "Comment on "elucidation of charge-transfer sers selection rules by considering the excited state properties and the role of electrode potential" by m. mohammadpour, m. h. khodabandeh, l. visscher and z. jamshidi, phys. chem. chem. phys., 2017, 19, 7833," Phys. Chem. Chem. Phys. **19**, 27888–27891 (2017).

[269]C. Rhodes, S. Franzen, J.-P. Maria, M. Losego, D. N. Leonard, B. Laughlin, G. Duscher, and S. Weibel, "Surface plasmon resonance in conducting metal oxides," J. Appl. Phys. **100**, 054905

(2006).

[270]M. D. Losego, A. Y. Efremenko, C. L. Rhodes, M. G. Cerruti, S. Franzen, and J.-P. Maria, "Conductive oxide thin films: Model systems for understanding and controlling surface plasmon resonance," Journal of Applied Physics **106**, 024903 (2009).

[271]L. Li, T. Hutter, A. S. Finnemore, F. M. Huang, J. J. Baumberg, S. R. Elliott, U. Steiner, and S. Mahajan, "Metal oxide nanoparticle mediated enhanced raman scattering and its use in direct monitoring of interfacial chemical reactions," Nano Lett. **12**, 4242–4246 (2012).

[272]C. Ye, Y. Zhao, and W. Liang, "Resonance raman spectra of organic molecules absorbed on inorganic semiconducting surfaces: Contribution from both localized intramolecular excitation and intermolecular charge transfer excitation," J. Chem. Phys. **143**, 154105 (2015).

[273]D. Aranda, S. Valdivia, F. J. Avila, J. Soto, J. C. Otero, and I. López-Tocón, "Charge transfer at the nanoscale and the role of the out-of-plane vibrations in the selection rules of surface-enhanced raman scattering," Phys. Chem. Chem. Phys. **20**, 29430–29439 (2018).

[274]F. Avila, D. J. Fernandez, J. F. Arenas, J. C. Otero, and J. Soto, "Modelling the effect of the electrode potential on the metal–adsorbate surface states: relevant states in the charge transfer mechanism of sers," Chem. Commun. **47**, 4210–4212 (2011).

[275]F. Avila, C. Ruano, I. Lopez-Tocon, J. F. Arenas, J. Soto, and J. C. Otero, "How the electrode potential controls the selection rules of the charge transfer mechanism of sers," Chem. Commun. **47**, 4213–4215 (2011).

[276]G. Orlandi and F. Zerbetto, "Vibronic coupling in polyenes: The frequency increase of the active cc ag stretching mode in the absorption spectra," Chem. Phys. **108**, 187–195 (1986).

[277]N.-J. Kim, J. Kim, J.-B. Park, H. Kim, G.-C. Yi, and S. Yoon, "Direct observation of quantum tunnelling charge transfers between molecules and semiconductors for sers," Nanoscale **11**, 45–49 (2019).

[278]H.-Y. Shin, E.-L. Shim, Y.-J. Choi, J.-H. Park, and S. Yoon, "Giant enhancement of the raman response due to one-dimensional zno nanostructures," Nanoscale **6**, 14622–14626 (2014).

[279]L. Yang, W. Ruan, X. Jiang, B. Zhao, W. Xu, and J. R. Lombardi, "Contribution of zno to charge-transfer induced surface-enhanced raman scattering in au/zno/patp assembly," J. Phys. Chem. C **113**, 117–120 (2009).

[280]P. S. Londero, M. Leona, and J. R. Lombardi, "Definitive evidence for linked resonances in surface-enhanced raman scattering: Excitation profile of cu phthalocyanine," Appl. Phys. Lett. **102**, 111101 (2013).

[281]J. R. Lombardi and R. L. Birke, "Excitation profiles and the continuum in sers: Identification of fano line shapes," J. Phys. Chem. C **114**, 7812–7815 (2010).

[282]J. R. Lombardi, "The theory of surface-enhanced raman spectroscopy on organic semiconductors: J-aggregates," Chem. Phys. Lett. **751**, 137553 (2020).

[283]J. R. Lombardi, "Enhanced by organic surfaces," Nat. Mater. **16**, 878–880 (2017).

[284]R. Livingstone, X. Zhou, M. C. Tamargo, J. R. Lombardi, L. G. Quagliano, and F. Jean-Mary, "Surface enhanced raman spectroscopy of pyridine on cdse/znbese quantum dots grown by molecular beam epitaxy," J. Phys. Chem. C **114**, 17460–17464 (2010).

[285]S. Feng, M. C. dos Santos, B. R. Carvalho, R. Lv, Q. Li, K. Fujisawa, A. L. Elías, Y. Lei, N. Perea-López, M. Endo, M. Pan, M. A. Pimenta, and M. Terrones, "Ultrasensitive molecular sensor using n-doped graphene through enhanced raman scattering," Sci. Adv. **2**, e1600322 (2016).

[286]Y. Yin, P. Miao, Y. Zhang, J. Han, X. Zhang, Y. Gong, L. Gu, C. Xu, T. Yao, P. Xu, Y. Wang, B. Song, and S. Jin, "Significantly increased raman enhancement on mox2 (x = s, se) monolayers upon phase transition," Adv. Funct. Mater. **27**, 1606694 (2017).

[287]Z. Zheng, S. Cong, W. Gong, J. Xuan, G. Li, W. Lu, F. Geng, and Z. Zhao, "Semiconductor sers enhancement enabled by oxygen incorporation," Nat Commun. **8**, 1993 (2017).

[288]W. A. Shapley, J. R. Reimers, and N. S. Hush, "Indo/s parameters for gold," Int. J. Quantum Chem. **90**, 424–438 (2002).

[289]M. K. Nazeeruddin, Q. Wang, L. Cevey, V. Aranyos, P. Liska, E. Figgemeier, C. Klein, N. Hirata, S. Koops, S. A. Haque, J. R. Durrant, A. Hagfeldt, A. B. P. Lever, and M. Grätzel, "Dft-indo/s modeling of new high molar extinction coefficient charge-transfer sensitizers for solar cell applications," Inorganic Chemistry **45**, 787–797 (2006).

[290]T. Fox, M. Kotzian, and N. Roesch, "Design of rigid donor-acceptor systems with a low-lying charge-transfer state: an indo model study of barrelene-based compounds," J. Phys. Chem. **97**, 11420–11426 (1993).

[291]R. L. Gieseking, M. A. Ratner, and G. C. Schatz, "Implementation of indo/sci with cosmo implicit solvation and benchmarking for solvatochromic shifts," J. Phys. Chem. A **120**, 9878–9885 (2016).

[292]R. L. Gieseking, M. A. Ratner, and G. C. Schatz, "Semiempirical modeling of ag nanoclusters: New parameters for optical property studies enable determination of double excitation contributions to plasmonic excitation," J. Phys. Chem. A **120**, 4542–4549 (2016).

[293]R. L. M. Gieseking, M. A. Ratner, and G. C. Schatz, "Benchmarking semiempirical methods to compute electrochemical formal potentials," J. Phys. Chem. A **122**, 6809–6818 (2018).

[294]J. Soto, D. J. Fernández, S. P. Centeno, I. López Tocón, and J. C. Otero, "Surface orientation of pyrazine adsorbed on silver from the surface-enhanced raman scattering recorded at different electrode potentials," Langmuir **18**, 3100–3104 (2002).

[295]R. L. M. Gieseking, "Quantum mechanical effects in high-resolution tip-enhanced raman imaging," J. Phys. Chem. C **126**, 11690–11700 (2022).

[296]M. Galperin, M. A. Ratner, and A. Nitzan, "Raman scattering in current-carrying molecular junctions," J. Chem. Phys. **130**, 144109 (2009).

[297]M. Galperin and A. Nitzan, "Optical properties of current carrying molecular wires," J. Chem. Phys. **124**, 234709 (2006).

[298]M. Galperin and A. Nitzan, "Current-induced light emission and light-induced current in molecular-tunneling junctions," Phys. Rev. Lett. **95**, 206802 (2005).

[299]M. K. Schmidt, R. Esteban, A. González-Tudela, G. Giedke, and J. Aizpurua, "Quantum mechanical description of raman scattering from molecules in plasmonic cavities," ACS Nano **10**, 6291–6298 (2016).

[300]M. Kamandar Dezfouli and S. Hughes, "Quantum optics model of surface-enhanced raman spectroscopy for arbitrarily shaped plasmonic resonators," ACS Photonics **4**, 1245–1256 (2017).

[301]H. A. Kramers and W. Heisenberg, "Über die streuung von strahlung durch atome," Z. Phys. **31**, 681 (1925).

[302]P. A. M. Dirac, "The quantum theory of dispersion," Proc. R. Soc. Lond. A **114**, 710 (1927).

[303]A. C. Albrecht, ""forbidden" character in allowed electronic transitions," J. Chem. Phys. **33**, 156–169 (1960).

[304]A. C. Albrecht, "Vibronic calculations in benzene," J. Chem. Phys. **33**, 169–178 (1960).

[305]A. C. Albrecht, "On the theory of raman intensities," J. Chem. Phys. **34**, 1476–1484 (1961).

[306]S.-Y. Lee, "Placzek-type polarizability tensors for raman and resonance raman scattering," J. Chem. Phys. **78**, 723–734 (1983).

[307]J. M. Schulman and R. Detrano, "Semiclassical theory of vibrational raman intensities," Phys. Rev. A **10**, 1192–1197 (1974).

[308]C. D. Allemand, "Depolarization ratio measurements in raman spectrometry," Appl. Spectrosc. **24**, 348–353 (1970).

[309]S.-Y. Lee and E. J. Heller, "Time-dependent theory of raman scattering," J. Chem. Phys. **71**, 4777 (1979).

[310]S. Lee, "Semiclassical theory of radiation interacting with a molecule," J. Chem. Phys. **76**, 3064–3074 (1982).

[311]E. J. Heller, R. Sundberg, and D. Tannor, "Simple aspects of raman scattering," J. Phys. Chem. **86**, 1822 (1982).

[312]J. M. Schulman and W. S. Lee, "A polarizability theory of the resonance raman effect," J. Chem. Phys. **74**, 4930–4935 (1981).

[313]L. Jensen, L. L. Zhao, J. Autschbach, and G. C. Schatz, "Theory and method for calculating resonance Raman scattering from resonance polarizability derivatives," J. Chem. Phys. **123**, 174110 (2005).

[314]L. Jensen, J. Autschbach, and G. C. Schatz, "Finite lifetime effects on the polarizability within time-dependent density-functional theory," J. Chem. Phys. **122**, 224115 (2005).

[315]D. Rappoport, S. Shim, and A. Aspuru-Guzik, "Simplified sum-over-states approach for predicting resonance raman spectra. application to nucleic acid bases," J. Phys. Chem. Lett. **2**, 1254, 1260 (2011).

[316]S. Corni and J. Tomasi, "Enhanced response properties of a chromophore physisorbed on a metal particle," J. Chem. Phys. **114**, 3739–3751 (2001).

[317]S. Jørgensen, M. A. Ratner, and K. V. Mikkelsen, "Heterogeneous solvation: An ab initio approach," J. Chem. Phys. **115**, 3792–3803 (2001).

[318]S. Corni and J. Tomasi, "Surface enhanced raman scattering from a single molecule adsorbed on a metal particle aggregate: A theoretical study," J. Chem. Phys. **116**, 1156–1164 (2002).

[319]S. Corni and J. Tomasi, "Excitation energies of a molecule close to a metal surface," J. Chem. Phys. **117**, 7266–7278 (2002).

[320]D. Neuhauser and K. Lopata, "Molecular nanopolaritonics: Cross manipulation of near-field plasmons and molecules. i. theory and application to junction control," J. Chem. Phys. **127**, 154715 (2007).

[321]K. Lopata and D. Neuhauser, "Multiscale maxwell–schrödinger modeling: A split field finite-difference time-domain approach to molecular nanopolaritonics," J. Chem. Phys. **130**, 104707 (2009).

[322]D. J. Masiello and G. C. Schatz, "On the linear response and scattering of an interacting molecule-metal system," J. Chem. Phys. **132**, 064102 (2010).

[323]M. A. Watson, D. Rappoport, E. M. Y. Lee, R. Olivares-Amaya, and A. Aspuru-Guzik, "Electronic structure calculations in arbitrary electrostatic environments," J. Chem. Phys. **136**, 024101–14 (2012).

[324]S. Vukovic, S. Corni, and B. Mennucci, "Fluorescence enhancement of chromophores close to metal nanoparticles. optimal setup revealed by the polarizable continuum model," J. Phys. Chem. C **113**, 121–133 (2009).

[325]H. Chen, J. M. McMahon, M. A. Ratner, and G. C. Schatz, "Classical electrodynamics coupled to quantum mechanics for calculation of molecular optical properties: a rt-tddft/fdtd approach," J. Phys. Chem. C **114**, 14384–14392 (2010).

[326]V. Arcisauskaite, J. Kongsted, T. Hansen, and K. V. Mikkelsen, "Charge transfer excitation energies in pyridine-silver complexes studied by a qm/mm method," Chem. Phys. Lett. **470**, 285–288 (2009).

[327]D. J. Masiello and G. C. Schatz, "Many-body theory of surface-enhanced Raman scattering," Phys. Rev. A **78**, 042505 (2008).

[328]S. M. Morton and L. Jensen, "A discrete interaction model/quantum mechanical method for describing response properties of molecules adsorbed on metal nanoparticles," J. Chem. Phys. **133**, 074103 (2010).

[329]S. M. Morton and L. Jensen, "A discrete interaction model/quantum mechanical method to describe the interaction of metal nanoparticles and molecular absorption," J. Chem. Phys. **135**, 134103 (2011).

[330]J. L. Payton, S. M. Morton, J. E. Moore, and L. Jensen, "A discrete interaction model/quantum mechanical method for simulating surface-enhanced raman spectroscopy," J. Chem. Phys. **136**, 214103 (2012).

[331]J. C. Becca, X. Chen, and L. Jensen, "A discrete interaction model/quantum mechanical method for simulating surface-enhanced raman spectroscopy in solution," J. Chem. Phys. **154**, 224705 (2021).

[332]P. Liu, D. V. Chulhai, and L. Jensen, "Single-molecule imaging using atomistic near-field tip-enhanced raman spectroscopy," ACS Nano **11**, 5094–5102 (2017).

[333]D. V. Chulhai, X. Chen, and L. Jensen, "Simulating ensemble-averaged surface-enhanced raman scattering," J. Phys. Chem. C **120**, 20833–20842 (2016).

[334]J. L. Payton, S. M. Morton, J. E. Moore, and L. Jensen, "A hybrid atomistic electrodynamics–quantum mechanical approach for simulating surface-enhanced raman scattering," Acc. Chem.

Res. **47**, 88–99 (2014).

[335]U. N. Morzan, D. J. Alonso de Armiño, N. O. Foglia, F. Ramírez, M. C. González Lebrero, D. A. Scherlis, and D. A. Estrin, "Spectroscopy in complex environments from qm–mm simulations," Chem. Rev. **118**, 4071–4113 (2018).

[336]J. Sun, Z. Ding, Y. Yu, and W. Liang, "Nonlinear features of fano resonance: a qm/em study," Phys. Chem. Chem. Phys. **23**, 15994–16004 (2021).

[337]E. Coccia, J. Fregoni, C. A. Guido, M. Marsili, S. Pipolo, and S. Corni, "Hybrid theoretical models for molecular nanoplasmonics," J. Chem. Phys. **153**, 200901 (2020).

[338]A. K. Harshan, M. J. J. Bronson, and L. Jensen, "Local-field effects in linear response properties within a polarizable frozen density embedding method," J. Chem. Theor. Comput. **18**, 380–393 (2022).

[339]S. L. McCall and P. M. Platzman, "Raman scattering from chemisorbed molecules at surfaces," Phys. Rev. B **22**, 1660–1662 (1980).

[340]B. N. J. Persson, "Surface resistivity and vibrational damping in adsorbed layers," Phys. Rev. B **44**, 3277–3296 (1991).

[341]B. N. J. Persson, K. Zhao, and Z. Zhang, "Chemical contribution to surface-enhanced Raman scattering," Phys. Rev. Lett. **96**, 207401 (2006).

[342]R. Chen and L. Jensen, "Quantifying the enhancement mechanisms of surface-enhanced raman scattering using a raman bond model," The Journal of Chemical Physics **153**, 224704 (2020).

[343]R. Chen and L. Jensen, "Interpreting the chemical mechanism in sers using a raman bond model," J. Chem. Phys. **152**, 024126 (2020).

[344]C. Ran and J. Lasse, "Understanding chemical enhancements of surface-enhanced raman scattering using a raman bond model for extended systems," J. Chem. Phys. **157**, 184705 (2022).

[345]N. Ramos-Berdullas, D. López-Carballeira, M. Mandado, and I. Pérez-Juste, "Revisiting the mechanism and the influence of the excitation wavelength on the surface-enhanced raman scattering of the pyridine-ag20 system," Theor. Chem. Acc. **134**, 60 (2015).

[346]F. L. Hirshfeld, "Bonded-atom fragments for describing molecular charge densities," Theor. Chim. Acta **44**, 129–138 (1977).

[347]G. K. Laura Gagliardi, Roland Lindh, "Local properties of quantum chemical systems: The loprop approach," J. Chem. Phys. **121**, 4494–4500 (2004).

[348]L. Silberstein, "L. molecular refractivity and atomic interaction. ii," Philos. Mag. **33**, 521–533 (1917).

[349]B. Yang, G. Chen, A. Ghafoor, Y.-F. Zhang, X.-B. Zhang, H. Li, X.-R. Dong, R.-P. Wang, Y. Zhang, Y. Zhang, and Z.-C. Dong, "Chemical enhancement and quenching in single-molecule tip-enhanced raman spectroscopy," Angew. Chem., Int. Edit. , e202218799.